Generalized Locally Most Powerful Tests for Distributed Sparse Signal Detection

Abdolreza Mohammadi , *Member, IEEE*, Domenico Ciuonzo , *Senior Member, IEEE*, Ali Khazaee ,
and Pierluigi Salvo Rossi , *Senior Member, IEEE*

Abstract—In this paper we tackle distributed detection of a localized phenomenon of interest (POI) whose signature is sparse via a wireless sensor network. We assume that both the position and the emitted power of the POI are unknown, other than the sparsity degree associated to its signature. We consider two communication scenarios in which sensors send either (i) their compressed observations or (ii) a 1-bit quantization of them to the fusion center (FC). In the latter case, we consider non-ideal reporting channels between the sensors and the FC. We derive generalized (i.e. based on Davies' framework (Davies, 1977)) locally most powerful detectors for the considered problem with the aim of obtaining computationally-efficient fusion rules. Moreover, we obtain their asymptotic performance and, based on such result, we design the local quantization thresholds at the sensors by solving a 1-D optimization problem. Simulation results confirm the effectiveness of the proposed design and highlight only negligible performance loss with respect to counterparts based on the (more-complex) generalized likelihood ratio.

Index Terms—Asymptotic analysis, generalized LMP test, imperfect channel, sparse signal, wireless sensor network.

I. INTRODUCTION

DISTRIBUTED detection (DD) is one of the most important tasks in wireless sensor networks (WSNs) and has attracted much interest in the last decades [2]–[4]. In general, a WSN consists of several low-cost sensors usually subject to severe energy & bandwidth constraints. All sensors send their observations to a fusion center (FC) where the information is combined and a (potentially more accurate) final decision is made regarding the absence (presence) of a phenomenon of interest (POI). Because of energy & bandwidth caps of the WSN, each sensor quantizes its observations into one or more bits about the occurrence of a POI before reporting to the FC [5]–[8].

The problem of sparse signal reconstruction has received much attention in recent years with the development of compressive sensing (CS) [9], [10]. Indeed, under the CS framework, sparse signals can be accurately recovered from a small number of available measurements. However, other than the complete recovery, an interesting subject in this area is performing *inference tasks* from (compressively-sensed) sparse signals without the need for explicit reconstruction [11]. Since CS theory implies much lower measurements compared to Nyquist theory, "sparse inference" based on compressed measurements is also desirable in high-dimensional settings due to storage, communication, and computation efficiency. Accordingly, several works have appeared in recent years, each focusing on a specific task (e.g. [12], [13] and [14], for *detection*, *estimation* and *classification*, respectively).

In this context, the *detection problem* has been the most investigated, starting from the seminal works [12], [15], providing error bounds for the likelihood ratio (with either partial- or full-knowledge of the sparse signal to be detected). In the former case [12] a universal compressive matrix design was investigated, whereas in the latter case [15] subspace-knowledge of the sparse signal was leveraged to design an improved measurement matrix. Leveraging analogous sparsity knowledge at the detection stage, an enhanced locally most powerful (LMP) test was designed in [16] based on Padé approximation. Differently, detection of randomly-unknown sparse signals lying in lower-dimensional subspace was attempted in [17]. Based on alternative assumptions, the Bernoulli-Gaussian (BG) distribution was used to model (random) sparsity in [18] and a generalized likelihood ratio (GLR) test was proposed to deal with the unknown sparsity degree (via the Central Limit Theorem). Remarkably, the adaptive sensing [19] and sequential detection [20] setups were also tackled within the CS realm.

In recent years, more studies have been devoted to the use of (collaborative) CS techniques in networked data [33], [34], with many relevant works focusing on *DD of a sparse signal via WSNs*. In these works, the FC makes a global decision about the presence or absence of a sparse signal based on compressed measurements sent from different sensors [22], [24]–[26], [28]–[31], [35]. The DD problem of sparse signals (having a common sparsity support) in Gaussian noise from a sensor network is considered in [26] and a LMP test is proposed. In [24], the sparsity is modeled in a deterministic fashion (subspace assumption) and a GLR fusion rule is obtained based on the estimated sparsity support. Remarkably, fusion techniques for detecting

TABLE I
CATEGORIZATION OF CLOSELY-RELATED WORKS ON DISTRIBUTED DETECTION VIA WSNs. THE PAPERS ARE REPORTED IN CHRONOLOGICAL ORDER. ACRONYMS MEANING IS REPORTED AT THE BOTTOM OF THE TABLE

Author & Year	Venue	ST	SP–MOD	RC	Q	L–POI
A. Shoari *et al.*, 2012	*Proc. IEEE MILCOM* [21]	○	–	○	◐	●
H. Zayyani *et al.*, 2016	*IEEE Signal Process. Lett.* [22]	●	D	○	◑	○
D. Ciuonzo *et al.*, 2017	*ELSEVIER Inf. Fus.* [23]	○	–	●	◐	●
T. Wimalajeewa *et al.*, 2017	*IEEE Trans. Signal Inf. Process. Netw.* [24]	●	D	○	○	○
B. Kailkhura *et al.*, 2017	*IEEE Trans. Signal Process.* [25]	●	D + G	○	○	○
X. Wang *et al.*, 2018	*IEEE Signal Process. Lett.* [26]	●	BG	○	○	○
D. Ciuonzo *et al.*, 2018	*IEEE Wireless Comm. Letters* [27]	○	–	●	◐	●
X. Wang *et al.*, 2019	*IEEE Trans. Signal Process.* [28]	●	BG	○	◑	○
X. Wang *et al.*, 2019	*IEEE Trans. Signal Process.* [29]	●	BG	○	◑	○
C. Li *et al.*, 2019	*IEEE Signal Process. Lett.* [30]	●	BG	○	◐	○
C. Li *et al.*, 2020	*IEEE Trans. Signal Process.* [31]	●	BG	○	○	○
D. Ciuonzo *et al.*, 2021	*IEEE Internet Things J.* [32]	○	–	●	●	●
This Paper	—	●	BG	●	●	●

Legend:
ST (Signal Type): ○ (ordinary signals); ● (sparse signals).
SP–MOD (Sparsity Model): D (deterministic); G (Gaussian), BG (Bernoulli-Gaussian).
RC (Reporting Channels): ○ (ideal); ● (noisy).
Q (Quantization): ○ (no quantization); ◐ (raw quantization); ◑ (likelihood-ratio quantization) ● (both quantization types).
L-POI (Localized POI): ○ (no); ● (yes).

sparse signals via WSNs have been also designed by including physical-layer security guarantees in [25], [31]. Because of *bandwidth scarcity* in the network, compressed observations at the sensors should be quantized into one or multiple bits before sending to the FC. Accordingly, in [22] sparse signal detection in WSNs from one-bit CS-based measurements is performed, and a sign-GLR and a double-stage detector (leveraging binary iterative hard thresholding) are proposed to capitalize signal sparsity. In [28] the authors have investigated the LMP rule for detection of sparse signals with quantized observations in WSN, and the extension of the above design to the generalized Gaussian noise setup has been reported in [29]. More recently, the same DD problem has been also investigated for sensors quantizing their local likelihood ratios (in cases they can be computed) into 1-bit and reporting them to the FC for global decision [30]. All the above works on sparse signal DD consider an ideal channel between the FC and the sensors. However, due to their battery-powered nature, sensors need to enforce also *low-energy communications*. Hence, it is of practical importance considering *imperfect channels* between the sensors and the FC [23], [36], [37]. More important, though these works capitalize WSN diversity for "sparse" DD, *the aforementioned literature does not take into account that POIs localized in a compact space region (e.g. oil leakage, biological release) lead to uneven (distance-dependent) signal strength among the sensors*.

On the contrary, DD of a *localized POI* based on WSN-originated quantized measurements has been considered in [21], [23], where detectors based on either the GLR or the generalized LMP (and hybrid combinations of both) have been proposed. Aiming at further performance gains, (optimized) quantizer design for generalized LMP has been proposed in [27]. Recent studies dealing with this task also include multiplicative fading into the received signal, see e.g. [32]. Nonetheless, *none of the aforementioned works have addressed DD of localized POIs whose signature at each sensor node is modeled as sparse signals and CS plus quantization techniques are used at each node*.

Accordingly, in Table I we summarize the closely-related works on (i) DD of sparse signal(s) (column **ST**) and (ii) DD of a localized POI (column **L-POI**), so as to highlight the novelty of our work. When referring to DD works assuming a sparse signal, we also detail the peculiar sparsity model considered (column **SP-MOD**). The taxonomy also includes whether quantization (column **Q**) and non-ideal channels (column **RC**) were considered in the reporting phase of the sensor nodes. In the former case, the type(s) of quantization investigated is (are) also highlighted.

Accordingly, the *main contributions* of this work are summarized as follows:

- We address the DD of a POI measured as sparse signals by different sensors. The (average) path loss of each signal is modeled by a deterministic and unknown function depending on the sensor-event distance, called amplitude attenuation function (AAF) [23]. We use the Bernoulli-Gaussian distribution to model the sparse signal so that its average power depends on the AAF. Herein, we assume that the signal power (σ_s^2), the sparsity degree (ϵ) and the POI position ($\boldsymbol{y}_P$) are *all* unknown.
- We consider *two* communication scenarios. In the *first* case, each sensor sends its *full-precision* (compressed) observation to the FC through an ideal channel. This scenario

is taken as a desirable upper bound. Conversely, in the *second* scenario, each sensor *quantizes* either (*a*) the (raw) observation or (*b*) the corresponding likelihood ratio (LR) into a *single bit*. In the quantized case, to face realistic energy-budgets in WSNs, it is assumed the sensors send their bits to the FC via an imperfect reporting channel, modeled as a binary symmetric channel (BSC). Relevant BSC scenarios are time-based parallel-access channels (e.g. NB-IoT) where each sensor decision is decoded independently [32], [38] or multiple-access channels with a large-array at the FC where decoding is operated via a linear filter (to decouple sensors' contributions) and a sign-based logic [39].

- Given the considered DD model, we investigate *three hypothesis tests:* **S1**–the sparsity parameter is tested (σ_s^2 and $\boldsymbol{y}_P$ are considered as nuisances); **S2**–the POI power is tested (ϵ and $\boldsymbol{y}_P$ are considered as nuisances); **S3**–the product of the sparsity parameter and the POI power is tested ($\boldsymbol{y}_P$ is considered as a nuisance).

- Since there are nuisance parameters present only under the alternative hypothesis, the (standard) LMP rule is not applicable here. Therefore, we use a *generalized* version of the LMP rule resorting to Davies technique [1], shortly denoted as DLMP rule in this work. The aim is the design of an efficient fusion rule as opposed to the usual (but more cumbersome) GLR-based rules. This applies to (I) each test and (II) both communication scenarios (analog vs. quantized) considered.

- By exploiting a remarkable property of the LMP rule when considering its (position-clairvoyant) asymptotic performance, we are able to design the quantization thresholds for each sensor according to this rationale, for both raw-quantization (RQ) and LR-quantization (LQ) cases.

- Numerical results are provided to investigate the performance of DLMP rules in comparison to GLR-based counterparts (derived for the same problem) for a relevant range of WSN system & sensing parameters.

For convenience, we provide the list of acronyms employed throughout this paper in Table II . The rest of the paper is organized as follows. Section II provides an overview of the system model and the problem statement. In Section III, a fusion rule based on the DLMP test is derived when the sensors send their full-precision observation to the FC. In Section IV, we obtain rules using DLMP test based on the 1-bit quantized data. In Section IV-D, by using the asymptotic analysis of the statistics of the detectors, we obtain the quantization threshold for each sensor. In Section V, simulation results are presented to evaluate the performance of the proposed detectors. Conclusions are drawn in Section VI, along with potential future directions.[1]

---

[1]**Notations:** Lower-case (resp. upper-case) bold letters denote vectors (resp. matrices), with a_k (resp. $a_{n,m}$) representing the kth element (resp. (n, m)th element) of a (resp. $\mathbf{A}$); upper-case calligraphic letters, e.g. $\mathcal{A}$, denote finite sets; $\mathbb{R}$ denotes set of real numbers; $(\cdot)^T$, $\mathbb{E}\{\cdot\}$ and $\|\cdot\|$ denote transpose, expectation and vector Euclidean norm operators, respectively; $u(\cdot)$ and $\delta(\cdot)$ denote Heaviside (unit) step and Dirac delta functions, respectively; the symbols $\sim$ and $\overset{a}{\sim}$ mean "distributed as" and "asymptotically distributed as"; $p(\cdot)$ (resp. $P(\cdot)$) represents probability density (resp. mass) functions; $x \sim \mathcal{N}(m, \sigma^2)$

TABLE II
LIST OF ACRONYMS USED THROUGHOUT THE MANUSCRIPT.

Acronym	Definition
AAF	Amplitude attenuation function
BEP	Bit error probability
BG	Bernoulli-Gaussian
BSC	Binary symmetric channel
CS	Compressive sensing
DD	Distributed detection
(D)LMP	(Davies) locally most powerful
EL	Exponential-law
FC	Fusion center
GLR	Generalized likelihood ratio
LQ	Likelihood quantization
LR	Likelihood ratio
ML	Maximum likelihood
PL	Power-law
POI	Phenomenon of interest
ROI	Region of interest
RQ	Raw quantization
ROC	Receiver operating characteristic
UMP	Uniformly most powerful
WSN	Wireless sensor network

II. PROBLEM STATEMENT

In this work, we consider the DD problem of a localized POI generating *sparse signals* lying in a K-dimensional space (e.g. time- or frequency-domain). We assume that the signal is generated by a POI within a monitored region of interest (ROI), denoted with $\mathcal{A}$. The WSN consists of M spatially-distributed sensors indexed by $\{m = 1, \ldots, M\}$ with parallel topology in which each sensor sends its data to an FC for global decision. The overall model is summarized in Fig. 1. In the following of this section, we detail the DD problem and the related background.

A. System Model

The detection task based on the compressed measurement for the mth sensor can be represented by a binary hypothesis test as follows:

$$\begin{cases} \mathcal{H}_0: & x_m = n_m, \\ \mathcal{H}_1: & x_m = \boldsymbol{h}_m^T \boldsymbol{s}_m\, d\left(\boldsymbol{y}_P, \boldsymbol{y}_m\right) + n_m, \end{cases} \tag{1}$$

where $\mathcal{H}_0$ and $\mathcal{H}_1$ are the hypotheses corresponding to the absence and the presence of the POI, respectively. Herein, $x_m \in \mathbb{R}$ is the compressed measurement, $\boldsymbol{h}_m \in \mathbb{R}^{K \times 1}$ represents the known measurement vector independent of the signals [26], [28] and $n_m \sim \mathcal{N}(0, \sigma_{\mathrm{n},m}^2)$ denotes the zero-mean Gaussian noise with known variance. The noise terms n_m are assumed statistically independent over space (viz. sensors). Also, $\boldsymbol{s}_m \in \mathbb{R}^{K \times 1}$ represents the sparse signal measured at mth sensor containing a *few* dominant elements, as detailed in later Section II-B.

---

indicates a Gaussian random variable with mean m and variance σ^2; $p_{\mathcal{N}}(\cdot)$ and $\mathcal{Q}(\cdot)$ denote the pdf and the tail probability of a zero-mean unit-variance Gaussian random variable, i.e. $\mathcal{Q}(x) = \int_x^\infty \frac{1}{\sqrt{2\pi}} \exp(-\frac{t^2}{2}) dt$.
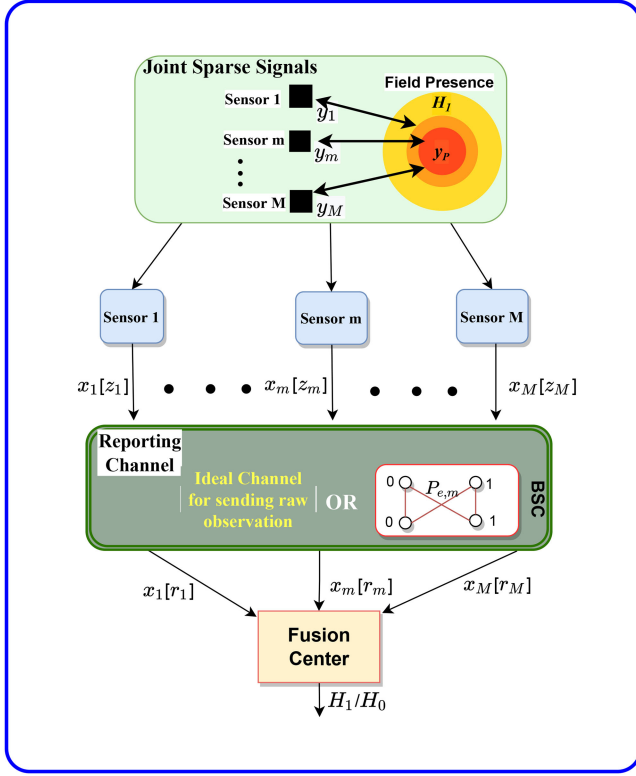
Fig. 1. The system model used in this paper. Each compressed observation (resp. each bit arising from compression and quantization) is sent through an ideal channel (resp. a BSC) and received by the FC.

Moreover, $\boldsymbol{y}_m \in \mathbb{R}^d$ denotes the *known* mth sensor position, whereas $\boldsymbol{y}_P \in \mathbb{R}^d$ represents the *unknown* POI position. The term $d(\boldsymbol{y}_P, \boldsymbol{y}_m)$ denotes the AAF, which models the (average) signal strength decay at the generic sensor. Indeed, the AAF depends on the sensor-POI distance $\|\boldsymbol{y}_P - \boldsymbol{y}_m\|$ and reflects the fact that high-SNR (resp. low-SNR) observations usually correspond to sensors closer to (resp. farther from) the POI.

In this paper, we utilize *two* relevant attenuation models, namely the *power-law* (PL) model

$$d(\boldsymbol{y}_P, \boldsymbol{y}_m) \triangleq \frac{1}{\sqrt{1 + (\|\boldsymbol{y}_P - \boldsymbol{y}_m\| / \beta)^\alpha}}, \quad (2)$$

and the *exponential-law* (EL) model

$$d(\boldsymbol{y}_P, \boldsymbol{y}_m) \triangleq \sqrt{\exp\left(-\|\boldsymbol{y}_P - \boldsymbol{y}_m\|^2 / \beta^2\right)}, \quad (3)$$

as deterministic AAFs [23], [27], [32]. The terms α and β in (2) and (3) are the decay exponent and POI (approximate) extent, respectively.

B. Signal Model

Herein, we assume that the sparse signals measured by different sensors $\{\boldsymbol{s}_m, m = 1, 2, \ldots, M\}$ share the same $K \times 1$ binary-valued sparsity pattern $\boldsymbol{v}$ [28], [29], namely

$$\begin{cases} v_k = 1, & \text{if } \{s_{m,k} \neq 0, m = 1, 2, \ldots, M\} \\ v_k = 0, & \text{if } \{s_{m,k} = 0, m = 1, 2, \ldots, M\}, \end{cases} \quad (4)$$

for $k = 1, \ldots, K$. In other words, the non-zero entries in the sparse signals $\boldsymbol{s}_m$'s have the *same locations*, while they may have different values for different sensors.

Although different modeling choices can be pursued for the sparse signals (see e.g. Table I), herein we resort to a (probabilistic) BG model. The latter has been extensively used in several studies to model sparse signals (including DD setups) [18], [26], [28], [40]–[42] and shown to fit several practical scenarios, including gene factor analysis [43], electromagnetic imaging of metallic reflectors [44], and spectral analysis of astrophysical data [45].

To model the sparse signal using BG distribution in this paper, we assume that the entries in $\boldsymbol{v}$ are independent and identically distributed (i.i.d.) random variables according to a Bernoulli probability mass function (pmf), i.e. $v_k = 1$ (resp. $v_k = 0$) with probability ϵ (resp. $(1 - \epsilon)$). The parameter $0 \leq \epsilon \leq 1$ models the sparsity degree of the signals [18], [26]. Likewise, it is assumed that all the nonzero elements of the sparse signals $\{\boldsymbol{s}_m, m = 1, 2, \ldots, M\}$ are i.i.d. random variables with Gaussian distribution, i.e. $\mathcal{N}(0, \sigma_s^2)$ [26]. In other words, Bernoulli random variables with probability ϵ are associated to the position of the non-zero values of the sparse signal, and the corresponding values follow a zero-mean Gaussian distribution with variance σ_s^2 [40].

Accordingly, the BG distribution for kth entry of mth sensor can be written as [26], [46]

$$s_{m,k} \sim \epsilon \mathcal{N}(0, \sigma_s^2) + (1 - \epsilon)\,\delta(s_{m,k}) \quad \forall m, \forall k \quad (5)$$

i.e. as a mixture (weighted by ϵ) of a delta function (centered in zero) and a Gaussian distribution. In this work, we *do not make any restrictive assumption* regarding the knowledge of σ_s^2 and ϵ, i.e. we assume that *both* parameters are *unknown*. From (1), the probability density function (pdf) of observation of mth sensor node can be obtained as follows:

$$\begin{cases} x_m \sim \mathcal{N}(0, \sigma_{\mathrm{n},m}^2), & \text{under } \mathcal{H}_0 \\ x_m \overset{a}{\sim} \mathcal{N}\left(0, \epsilon\,\sigma_s^2\,\|\boldsymbol{h}_m\|^2\,d^2(\boldsymbol{y}_P, \boldsymbol{y}_m) + \sigma_{\mathrm{n},m}^2\right), & \text{under } \mathcal{H}_1 \end{cases} \quad (6)$$

for $m = 1, \ldots, M$. The asymptotic distribution of x_m under $\mathcal{H}_1$ has been derived in [18] by assuming that K is large and utilizing the Lyapunov Central Limit Theorem. For compactness, we collect all the sensors' measurements in $\boldsymbol{x} \triangleq [x_1, x_2, \ldots, x_M]^T$. Also, we define the mth equivalent variance as $\sigma_m^2(\epsilon, \sigma_s^2, \boldsymbol{y}_P) \triangleq (\epsilon\,\sigma_s^2\,\|\boldsymbol{h}_m\|^2\,d^2(\boldsymbol{y}_P, \boldsymbol{y}_m) + \sigma_{\mathrm{n},m}^2)$, which will be used hereinafter.

C. Hypothesis Testing Scenarios Considered

The DD problem in this work can be considered as a one-sided hypothesis testing problem in *three* different scenarios **S1-S3**, detailed as follows:

■**S1**: we test the *unknown* sparsity degree ϵ. Accordingly, the sparsity degree equals zero under $\mathcal{H}_0$, whereas it is positive under $\mathcal{H}_1$. Our analysis will focus on the case where $\epsilon \to 0$ under $\mathcal{H}_1$ which results in a *low-sparsity* POI detection. Based on the signal model in this paper, the problem of detection of sparse signal leads to the following binary hypothesis

test problem [28]:

$$\begin{cases} \mathcal{H}_0: & \epsilon = 0 \\ \mathcal{H}_1: & \epsilon > 0, \quad \{\sigma_s^2, \boldsymbol{y}_P\} \text{ (nuisances)} \end{cases} \tag{7}$$

which is a one-sided and close hypothesis test problem.

■**S2**: we test the *unknown* POI power σ_s^2. Accordingly, the POI power equals zero under $\mathcal{H}_0$, whereas it is positive under $\mathcal{H}_1$. Our analysis will focus on the case where $\sigma_s^2 \to 0$ under $\mathcal{H}_1$, which results in a *low-power* POI detection.

This assumption leads to the following one-sided and close hypothesis test:

$$\begin{cases} \mathcal{H}_0: & \sigma_s^2 = 0 \\ \mathcal{H}_1: & \sigma_s^2 > 0, \quad \{\epsilon, \boldsymbol{y}_P\} \text{ (nuisances)} \end{cases} \tag{8}$$

■**S3**: we test the *unknown* product of the sparsity degree and the POI power, i.e. $\kappa \triangleq \epsilon \cdot \sigma_s^2$. Accordingly, the aforementioned product equals zero under $\mathcal{H}_0$, whereas it is positive under $\mathcal{H}_1$. Our analysis will focus on the case where $\kappa \to 0$ under $\mathcal{H}_1$, which results in a *low-power/low-sparsity* POI detection. This assumption leads to the following one-sided hypothesis test:

$$\begin{cases} \mathcal{H}_0: & \kappa = 0 \\ \mathcal{H}_1: & \kappa > 0, \quad \boldsymbol{y}_P \text{ (nuisance)} \end{cases} \tag{9}$$

Next subsection will lie the basis for the design of suitable fusion rules for the three scenarios considered. This is tantamount to the design of a statistic Λ (which is function of $\boldsymbol{x}$ or a compressed version in the quantized case) deciding in favor of $\mathcal{H}_1$ (resp. $\mathcal{H}_0$) when its value is above (resp. below) the threshold γ_{fc}.

Accordingly, we *evaluate the performance* of the fusion rules in terms of the well-known detection ($P_D \triangleq \Pr\{\Lambda > \gamma_{\text{fc}} | \mathcal{H}_1\}$, i.e. the complement of type II error) and false-alarm probabilities ($P_F \triangleq \Pr\{\Lambda > \gamma_{\text{fc}} | \mathcal{H}_0\}$, i.e. the type I error).

D. Generalized Locally Most Powerful Tests

The optimal detection performance is provided by the uniformly most powerful (UMP) test, which unfortunately does not exist for (general) one-sided hypothesis tests with vector-valued sufficient statistics [47]. In absence of the UMP test, the LMP test (also known as locally-optimum detector) has been extensively used in DD literature due to its simplicity and flexibility [48], [49].

The LMP test is an asymptotic version of the UMP test for one-sided and close hypothesis testing problems [50], namely $\mathcal{H}_0: \theta = \theta_0$ against $\mathcal{H}_1: \theta > \theta_0$, where $(\theta - \theta_0) \to 0$. Indeed the LMP test is obtained as the maximizer of the detection probability slope at θ_0 under a fixed value of false-alarm probability (i.e. as a generalization of the Neyman-Pearson lemma), see e.g. [2], [47], [51]. Additionally, the LMP test does not require an estimate of θ as opposed to the GLR test.

The LMP statistic can be obtained as the first-order Taylor expansion of the log-likelihood around the point $\theta = \theta_0$,

namely [50]:

$$\Lambda_{\text{LMP}} \triangleq \left(\frac{\partial \ln p\,(\,\cdot\,;\theta)}{\partial \theta} \right) \Bigg|_{\theta=\theta_0} \times \frac{1}{\sqrt{\mathcal{I}\,(\theta_0)}}, \tag{10}$$

where $p(\cdot;\theta)$ denotes the generic likelihood of the data versus θ and $\mathcal{I}(\cdot)$ represents the Fisher information. The latter, when evaluated at θ_0, is defined as:

$$\mathcal{I}\,(\theta_0) \triangleq \mathbb{E}\left\{ \left(\frac{\partial \ln p\,(\,\cdot\,;\theta)}{\partial \theta} \Bigg|_{\theta=\theta_0} \right)^2 \right\} \tag{11}$$

However, because of the nuisance parameters in the (one-sided) tests associated to scenarios **S1-S3** (cf. (7), (8), and (9)), the standard LMP test *is not applicable*. Additionally, the nuisance parameters in **S1-S3** are observable *only* under the alternative hypothesis $\mathcal{H}_1$.

In other terms, we are faced to test the general *one-sided* binary hypothesis test

$$\begin{cases} \mathcal{H}_0: & \theta = \theta_0 \\ \mathcal{H}_1: & \theta > \theta_0, \quad \boldsymbol{\rho} \text{ (nuisance)}, \end{cases} \tag{12}$$

where $\boldsymbol{\rho}$ is a nuisance vector parameter present only under $\mathcal{H}_1$, i.e. the pdf/pmf of the observations *does not depend* on $\boldsymbol{\rho}$ when $\mathcal{H}_0$ holds. For this reason, *generalized* LMP tests [23] have been proposed to solve the test of hypotheses specified in (12), based on Davies technique [1], as described hereinafter.

Suppose that, for *known* $\boldsymbol{\rho}$, $S(\boldsymbol{\rho})$ is an appropriate decision statistic such that $\mathcal{H}_1$ is declared if $S(\boldsymbol{\rho}) > b$, where b is a suitable threshold. For *unknown* $\boldsymbol{\rho}$, Davies proposed a test statistic Ω based on $S(\boldsymbol{\rho})$, namely $\Omega \triangleq \sup_{\boldsymbol{\rho} \in \mathcal{P}} S(\boldsymbol{\rho})$, where $\mathcal{P}$ denotes the nuisance parameter space.

Assuming that $S(\boldsymbol{\rho})$ is chosen as the LMP statistic, Davies LMP (DLMP) fusion rule is given by:

$$\Lambda_{\text{DLMP}} \triangleq \sup_{\boldsymbol{\rho} \in \mathcal{P}} \Lambda_{\text{LMP}}(\boldsymbol{\rho}). \tag{13}$$

The above statistic will be used in this work by considering the relevant signal parameter θ as ϵ, σ_s^2 or κ, depending on the scenario considered. Conversely, the relevant nuisance vector parameter will *always* include the POI position (namely $\{\sigma_s^2, \boldsymbol{y}_P\}$, $\{\epsilon, \boldsymbol{y}_P\}$ and $\{\boldsymbol{y}_P\}$ for **S1**, **S2** and **S3**, respectively).

III. GENERALIZED LMP DETECTOR USING THE RAW OBSERVATIONS

This section devises DLMP detectors for the three scenarios described in Section II-C. These detectors are based on the raw measurement vector $\boldsymbol{x}$, namely $\Lambda(\boldsymbol{x})$. The considered setup well suits to sensors *not* subject to strict (bandwidth & energy) constraints. Accordingly, the performance of the detectors obtained provides a practical upper-bound on achievable performance in the quantized case. The section is concluded with a comparison with the GLR for the same problem and the corresponding implementation aspects.

A. First Scenario (S1)

In this scenario, we test the sparsity degree ϵ associated to the POI. The corresponding DLMP detector (shortly denoted with DLMP-1) is written as:

$$\Lambda_{\text{DLMP}(1)} \triangleq \sup_{(\sigma_s^2, \boldsymbol{y}_P)} \frac{\left(\frac{\partial \ln p(\boldsymbol{x}; \epsilon, \sigma_s^2, \boldsymbol{y}_P)}{\partial \epsilon} \right) \Big|_{\epsilon=0}}{\sqrt{\mathcal{I}(\epsilon=0; \sigma_s^2, \boldsymbol{y}_P)}}, \quad (14)$$

where $\mathcal{I}(\epsilon; \sigma_s^2, \boldsymbol{y}_P)$ is the Fisher information assuming the pair $(\sigma_s^2, \boldsymbol{y}_P)$ *known*. The latter is given by:

$$\mathcal{I}\left(\epsilon; \sigma_s^2, \boldsymbol{y}_P\right) = \mathbb{E}\left\{ \left(\frac{\partial \ln p\left(\boldsymbol{x}; \epsilon, \sigma_s^2, \boldsymbol{y}_P\right)}{\partial \epsilon} \right)^2 \right\} \quad (15)$$

To derive the DLMP-1 statistic, the partial derivative of the log-likelihood with respect to (w.r.t.) ϵ is obtained as

$$\frac{\partial \ln p\left(\boldsymbol{x}; \epsilon, \sigma_s^2, \boldsymbol{y}_P\right)}{\partial \epsilon} =$$

$$\frac{\sigma_s^2}{2} \sum_{m=1}^{M} \left[\frac{x_m^2 \|\boldsymbol{h}_m\|^2 d^2\left(\boldsymbol{y}_P, \boldsymbol{y}_m\right)}{\sigma_m^4\left(\epsilon, \sigma_s^2, \boldsymbol{y}_P\right)} - \frac{\|\boldsymbol{h}_m\|^2 d^2\left(\boldsymbol{y}_P, \boldsymbol{y}_m\right)}{\sigma_m^2\left(\epsilon, \sigma_s^2, \boldsymbol{y}_P\right)} \right], \quad (16)$$

and the Fisher information is expressed in explicit form as

$$\mathcal{I}\left(\epsilon; \sigma_s^2, \boldsymbol{y}_P\right) = \frac{\sigma_s^4}{2} \sum_{m=1}^{M} \frac{\|\boldsymbol{h}_m\|^4 d^4\left(\boldsymbol{y}_P, \boldsymbol{y}_m\right)}{\sigma_m^4\left(\epsilon, \sigma_s^2, \boldsymbol{y}_P\right)} \quad (17)$$

Therefore, the DLMP-1 detector is obtained as follows:

$$\Lambda_{\text{DLMP}(1)} = \sup_{\boldsymbol{y}_P} \frac{\sum_{m=1}^{M} \|\boldsymbol{h}_m\|^2 d^2\left(\boldsymbol{y}_P, \boldsymbol{y}_m\right)\left(x_m^2 - \sigma_{\text{n},m}^2\right)}{\sqrt{\sum_{m=1}^{M} \|\boldsymbol{h}_m\|^4 d^4\left(\boldsymbol{y}_P, \boldsymbol{y}_m\right)}} \quad (18)$$

It is apparent that the DLMP-1 detector *does not depend* on the variance σ_s^2. Accordingly, the maximization is only carried out w.r.t. the POI position $\boldsymbol{y}_P$.

B. Second Scenario (S2)

In this scenario, we test the POI power σ_s^2. Therefore, the DLMP-2 detector is obtained as follows:

$$\Lambda_{\text{DLMP}(2)} = \sup_{(\epsilon, \boldsymbol{y}_P)} \frac{\left(\frac{\partial \ln p(\boldsymbol{x}; \epsilon, \sigma_s^2, \boldsymbol{y}_P)}{\partial \sigma_s^2} \right) \Big|_{\sigma_s^2=0}}{\sqrt{\mathcal{I}(\sigma_s^2 = 0; \epsilon, \boldsymbol{y}_P)}}, \quad (19)$$

where $\mathcal{I}(\sigma_s^2; \epsilon, \boldsymbol{y}_P)$ is the Fisher information assuming the pair $(\epsilon, \boldsymbol{y}_P)$ *known*. The latter is given by:

$$\mathcal{I}\left(\sigma_s^2; \epsilon, \boldsymbol{y}_P\right) = \mathbb{E}\left\{ \left(\frac{\partial \ln p\left(\boldsymbol{x}; \epsilon, \sigma_s^2, \boldsymbol{y}_P\right)}{\partial \sigma_s^2} \right)^2 \right\} \quad (20)$$

To derive the DLMP-2 statistic, the partial derivative of the log-likelihood w.r.t. σ_s^2 is obtained as:

$$\frac{\partial \ln p\left(\boldsymbol{x}; \epsilon, \sigma_s^2, \boldsymbol{y}_P\right)}{\partial \sigma_s^2} =$$

$$\frac{\epsilon}{2} \sum_{m=1}^{M} \left[\frac{x_m^2 \|\boldsymbol{h}_m\|^2 d^2\left(\boldsymbol{y}_P, \boldsymbol{y}_m\right)}{\sigma_m^4\left(\epsilon, \sigma_s^2, \boldsymbol{y}_P\right)} - \frac{\|\boldsymbol{h}_m\|^2 d^2\left(\boldsymbol{y}_P, \boldsymbol{y}_m\right)}{\sigma_m^2\left(\epsilon, \sigma_s^2, \boldsymbol{y}_P\right)} \right], \quad (21)$$

Conversely, the Fisher information can be obtained as follows:

$$\mathcal{I}\left(\sigma_s^2; \epsilon, \boldsymbol{y}_P\right) = \frac{\epsilon^2}{2} \sum_{m=1}^{M} \frac{\|\boldsymbol{h}_m\|^4 d^4\left(\boldsymbol{y}_P, \boldsymbol{y}_m\right)}{\sigma_m^4\left(\epsilon, \sigma_s^2, \boldsymbol{y}_P\right)} \quad (22)$$

By evaluating (19), it is easy to verify that the DLMP-2 statistic coincides with the DMLP-1 obtained in (18). Indeed, since the ratio in (19) is *independent* of ϵ, the optimization needs to be only performed w.r.t. $\boldsymbol{y}_P$.

C. Third Scenario (S3)

In this scenario, we test the product of the POI power and the sparsity degree $\kappa = \epsilon \cdot \sigma_s^2$. In such a case, the DLMP-3 detector is obtained as follows:

$$\Lambda_{\text{DLMP}(3)} = \sup_{\boldsymbol{y}_P} \frac{\left(\frac{\partial \ln p(\boldsymbol{x}; \kappa, \boldsymbol{y}_P)}{\partial \kappa} \right) \Big|_{\kappa=0}}{\sqrt{\mathcal{I}(\kappa = 0; \boldsymbol{y}_P)}}, \quad (23)$$

where $\mathcal{I}(\kappa; \boldsymbol{y}_P)$ is the Fisher information assuming $\boldsymbol{y}_P$ known. The latter is given by:

$$\mathcal{I}\left(\kappa; \boldsymbol{y}_P\right) = \mathbb{E}\left\{ \left(\frac{\partial \ln p\left(\boldsymbol{x}; \kappa, \boldsymbol{y}_P\right)}{\partial \kappa} \right)^2 \right\} \quad (24)$$

To derive the DLMP-3 statistic, the partial derivative of the log-likelihood w.r.t. κ is obtained as:

$$\frac{\partial \ln p\left(\boldsymbol{x}; \kappa, \boldsymbol{y}_P\right)}{\partial \kappa} =$$

$$\frac{1}{2} \sum_{m=1}^{M} \left[\frac{x_m^2 \|\boldsymbol{h}_m\|^2 d^2\left(\boldsymbol{y}_P, \boldsymbol{y}_m\right)}{\sigma_m^4\left(\epsilon, \sigma_s^2, \boldsymbol{y}_P\right)} - \frac{\|\boldsymbol{h}_m\|^2 d^2\left(\boldsymbol{y}_P, \boldsymbol{y}_m\right)}{\sigma_m^2\left(\epsilon, \sigma_s^2, \boldsymbol{y}_P\right)} \right], \quad (25)$$

Conversely, the Fisher information can be obtained as follows:

$$\mathcal{I}\left(\kappa; \boldsymbol{y}_P\right) = \frac{1}{2} \sum_{m=1}^{M} \frac{\|\boldsymbol{h}_m\|^4 d^4\left(\boldsymbol{y}_P, \boldsymbol{y}_m\right)}{\sigma_m^4\left(\kappa, \boldsymbol{y}_P\right)} \quad (26)$$

It is readily shown that applying the Davies method in this scenario leads to a detector which statistically *coincides* with DLMP1/2 detectors (see e.g. (18) for S1 scenario). The above result highlights that the DLMP detector is expected to perform well in the cases of (*i*) low-power ($\sigma_s^2 \to 0$), (*ii*) low-sparsity ($\epsilon \to 0$) and low-sparsity × power ($\kappa \to 0$). Indeed, if $\boldsymbol{y}_P$ were known, the above detector would represent the LMP statistic in *all* the three scenarios.

D. Comparison With GLR and Implementation Aspects

The obtained DLMP fusion rule reported in (18) can be implemented by performing a *grid search* w.r.t. $\boldsymbol{y}_P$ over the (limited) ROI $\mathcal{A} \in \mathbb{R}^d$. In other words, considering that the allowable values of the POI position $\boldsymbol{y}_P$ lie in the limited set $\mathcal{A} \subset \mathbb{R}^d$, the search space of $\boldsymbol{y}_P$ is then divided into C_P cells

with center equal to $\boldsymbol{y}_P[j]$, $j \in \{1, 2, \ldots, C_P\}$. Denoting with Λ_{DLMP} the DLMP-based statistic, we can *approximate* it (by discretization) as follows:

$$\Lambda_{\mathrm{DLMP}}(\boldsymbol{x}) \approx \max_{j=1,2,\ldots,C_P} \Lambda_{\mathrm{LMP}}(\boldsymbol{x}, \boldsymbol{y}_P[j]) \qquad (27)$$

Accordingly, the complexity DLMP-based fusion rule is $\mathcal{O}(M\,C_P)$. This implies a significant reduction with respect to the corresponding GLR-based counterpart, which represents the most common approach to deal with composite hypothesis tests. Indeed, in the latter case [50], its implicit expression is given by

$$\Lambda_{\mathrm{GLR}}(\boldsymbol{x}) \triangleq 2 \ln \left[\frac{p(\boldsymbol{x}; \hat{\kappa}, \widehat{\boldsymbol{y}}_P)}{p(\boldsymbol{x}; \kappa = 0)} \right]. \qquad (28)$$

In the above equation, the pair $(\hat{\kappa}, \widehat{\boldsymbol{y}}_P)$ represents the *maximum likelihood* (ML) *estimates* under $\mathcal{H}_1$, i.e.

$$(\hat{\kappa}, \widehat{\boldsymbol{y}}_P) \triangleq \arg \max_{(\kappa, \boldsymbol{y}_P)} p(\boldsymbol{x}; \kappa, \boldsymbol{y}_P). \qquad (29)$$

We observe that Λ_{GLR} requires the solution to an optimization task. Unfortunately, the ML estimate pair $(\hat{\kappa}, \widehat{\boldsymbol{y}}_P)$ cannot be obtained in closed form and this hinders its practical implementation. Hence, a (joint) grid approach is usually adopted on $(\kappa, \boldsymbol{y}_P)$, leading to a complexity equal to $\mathcal{O}(M\,C_P\,C_\kappa)$, where C_κ denotes the number of grid points associated to κ.

IV. GENERALIZED LMP TEST USING QUANTIZED DATA AND DESIGN OF THE QUANTIZER

Because of limited resources of energy and bandwidth in WSNs, we assume herein that the compressed observation at each sensor node x_m is also quantized into *one bit* via a deterministic quantizer. This is a common assumption usually employed in DD tasks, see e.g. [8], [46]. Then, each sensor sends one bit (associated to the presence or absence of the target) via an imperfect reporting channel, modeled as a BSC, to the FC. Therein a suitable and efficient fusion rule should employed to decide between $\mathcal{H}_0$ and $\mathcal{H}_1$ based on the (noisy) received bits from sensors. Due to the finite resolution nature of this setup, optimization of quantization thresholds at the sensors represents a degree of freedom to be leveraged to improve the fusion performance.

Accordingly, next subsections are devoted to (i) DD based on quantized raw observations (Section IV-A), named as raw quantization (RQ) and (ii) DD based on the quantized local LR (Section IV-B), named as likelihood quantization (LQ). Therein, similar to Section III (referring to the unlimited bandwidth/full-precision case), we consider the three scenarios introduced in Section II-C and we derive the DLMP fusion rule for each. The section proceeds with a qualitative comparison of the proposed rules with one-bit GLR counterparts (cf. Section IV-C). The section ends with design of the local quantizer (based on a sound rationale, cf. Section IV-D) in both the cases ($i - ii$).

A. Generalized LMP Test Using Quantized Raw Observation

Herein, we first assume that the compressed observation (x_m) at each sensor node is quantized into one bit via RQ, i.e. $z_m^{\mathrm{rq}} \triangleq u(x_m - \eta_m)$, where η_m denotes the corresponding quantizer

threshold. Given these assumptions, the probability that $z_m^{\mathrm{rq}} = 1$ under $\mathcal{H}_1$ is given by

$$\beta_m^{\mathrm{rq}}(\epsilon, \sigma_s^2, \boldsymbol{y}_P) \triangleq \mathcal{Q}\left(\eta_m / \sqrt{\sigma_m^2(\epsilon, \sigma_s^2, \boldsymbol{y}_P)}\right) \qquad (30)$$

whereas, when $\mathcal{H}_0$ holds, the above probability reduces to $\beta_{0,m}^{\mathrm{rq}} \triangleq \mathcal{Q}(\eta_m / \sqrt{\sigma_{\mathrm{n},m}^2})$.

Further, we assume that the quantized measurement z_m^{rq} is transmitted over a *non-ideal* reporting channel, here modeled as a BSC. As a result, the FC receives an error-prone r_m^{rq} from mth sensor node ($m = 1, \ldots, M$), which is given by:

$$r_m^{\mathrm{rq}} = \begin{cases} z_m^{\mathrm{rq}}, & \text{with probability } 1 - P_{e,m} \\ 1 - z_m^{\mathrm{rq}}, & \text{with probability } P_{e,m} \end{cases} \qquad (31)$$

where $P_{e,m}$ represents the (known) bit error probability (BEP) of the channel. The FC then forms the vector $\boldsymbol{r}^{\mathrm{rq}} \triangleq [r_1^{\mathrm{rq}}, r_2^{\mathrm{rq}}, \ldots, r_M^{\mathrm{rq}}]^T$ (i.e. based on the noisy received bits) and takes a global decision based on it. Given the above assumptions, the probability that $r_m^{\mathrm{rq}} = 1$ under $\mathcal{H}_1$ is

$$\alpha_m^{\mathrm{rq}}(\epsilon, \sigma_s^2, \boldsymbol{y}_P) =$$
$$(1 - P_{e,m})\, \beta_m^{\mathrm{rq}}(\epsilon, \sigma_s^2, \boldsymbol{y}_P) + P_{e,m}(1 - \beta_m^{\mathrm{rq}}(\epsilon, \sigma_s^2, \boldsymbol{y}_P)) \quad (32)$$

whereas, under $\mathcal{H}_0$, it holds $\alpha_{0,m}^{\mathrm{rq}} = (1 - P_{e,m})\, \beta_{0,m}^{\mathrm{rq}} + P_{e,m}(1 - \beta_{0,m}^{\mathrm{rq}})$.

For the considered RQ model, attempting to devise a DLMP for the cases **S1-S3** introduced in Section II-C leads to the *same fusion rule*, as shown by the following proposition.

Proposition 1: The one-bit DLMP fusion statistic based on RQ is coincident under the three different scenarios considered and equal to:

$$\Lambda_{\mathrm{1B-DLMP}}^{\mathrm{rq}} =$$
$$\sup_{\boldsymbol{y}_P} \frac{\sum_{m=1}^{M} (r_m^{\mathrm{rq}} - \alpha_{0,m}^{\mathrm{rq}})\, \Xi_m^{\mathrm{rq}}\, d^2(\boldsymbol{y}_P, \boldsymbol{y}_m)}{\sqrt{\sum_{m=1}^{M} \alpha_{0,m}^{\mathrm{rq}} \left[1 - \alpha_{0,m}^{\mathrm{rq}}\right] \left(\Xi_m^{\mathrm{rq}}\right)^2 d^4(\boldsymbol{y}_P, \boldsymbol{y}_m)}}, \qquad (33)$$

where the auxiliary definition

$$\Xi_m^{\mathrm{rq}} \triangleq \frac{(1 - 2P_{e,m})}{\alpha_{0,m}^{\mathrm{rq}} \left[1 - \alpha_{0,m}^{\mathrm{rq}}\right]} \frac{\eta_m}{\sigma_{\mathrm{n},m}^3}\, p_{\mathcal{N}}\left(\frac{\eta_m}{\sqrt{\sigma_{\mathrm{n},m}^2}}\right) \|\boldsymbol{h}_m\|^2 \quad (34)$$

has been employed.

Proof: The proof is given in Appendix A. ∎

Remarks: first of all, the above result complements the *coincidence* result obtained in the full-precision (infinite-bandwidth) case of Section III. Hence, also when RQ is employed at the sensors, the DLMP fusion statistic in (33) is expected to perform well in the cases of low-power ($\sigma_s^2 \to 0$), low-sparsity ($\epsilon \to 0$) and low-sparsity $\times$ power ($\kappa \to 0$). Finally, similarly to (18), the implementation of DLMP statistic requires *only* a maximization w.r.t. the POI position $\boldsymbol{y}_P$.

B. Generalized LMP Test Using Quantized LR

In this subsection, we use the 1-bit quantized local LRs to design the DLMP rule at the FC. Specifically, at the mth sensor,

the (local) LR can be written as follows:

$$\mathcal{L}_m = \frac{p\left(x_m; \epsilon, \sigma_s^2, \boldsymbol{y}_P\right)}{p\left(x_m; \mathcal{H}_0\right)}$$

$$= \sqrt{\frac{\sigma_{\text{n},m}^2}{\sigma_m^2\left(\epsilon, \sigma_s^2, \boldsymbol{y}_P\right)}} \exp\left(\frac{\epsilon\,\sigma_s^2\,\|\boldsymbol{h}_m\|^2}{2\,\sigma_{\text{n},m}^2\,\sigma_m^2\left(\epsilon, \sigma_s^2, \boldsymbol{y}_P\right)}\,x_m^2\right),$$
(35)

It can be easily observed that the LR is a *monotonically increasing function* of x_m^2 (or, equivalently $|x_m|$). This result holds independently on the unknown values $(\epsilon, \sigma_s^2, \boldsymbol{y}_P)$. Therefore, the local UMP detector at the mth sensor does exist and can be written, by Karlin-Rubin theorem [47], as:

$$z_m^{\text{lq}} = \begin{cases} 1, & \text{if } |x_m| \geq \tau_m \\ 0, & \text{if } |x_m| < \tau_m \end{cases}, \quad m = 1, \dots, M \qquad (36)$$

where τ_m is the quantization threshold to be determined. Given these assumptions, the probability that $z_m^{\text{lq}} = 1$ under $\mathcal{H}_1$ is given by

$$\beta_m^{\text{lq}}(\epsilon, \sigma_s^2, \boldsymbol{y}_P) \triangleq 2\,\mathcal{Q}\left(\tau_m \,/\, \sqrt{\sigma_m^2(\epsilon, \sigma_s^2, \boldsymbol{y}_P)}\right) \qquad (37)$$

whereas, when $\mathcal{H}_0$ holds, the above probability reduces to $\beta_{0,m}^{\text{lq}} \triangleq 2\,\mathcal{Q}(\tau_m/\sqrt{\sigma_{\text{n},m}^2})$.

As a result, the FC receives an error-prone r_m^{lq} from mth sensor node $(m = 1, \dots, M)$, which is given by:

$$r_m^{\text{lq}} = \begin{cases} z_m^{\text{lq}}, & \text{with probability } 1 - P_{e,m} \\ 1 - z_m^{\text{lq}}, & \text{with probability } P_{e,m} \end{cases} \qquad (38)$$

where $P_{e,m}$ represents the (known) BEP of the channel. Accordingly, z_m^{lq} is sent over a BSC and the FC receives r_m^{lq} based on (38) and forms $\boldsymbol{r}^{\text{lq}} \triangleq [r_1^{\text{lq}}, r_2^{\text{lq}}, \dots, r_M^{\text{lq}}]^T$.

Given these above assumptions, the probability that $r_m^{\text{lq}} = 1$ under $\mathcal{H}_1$ is given by $\alpha_m^{\text{lq}}(\epsilon, \sigma_s^2, \boldsymbol{y}_P) = (1 - P_{e,m})\,\beta_m^{\text{lq}}(\epsilon, \sigma_s^2, \boldsymbol{y}_P) + P_{e,m}(1 - \beta_m^{\text{lq}}(\epsilon, \sigma_s^2, \boldsymbol{y}_P))$ whereas under $\mathcal{H}_0$ it holds $\alpha_{0,m}^{\text{lq}} = (1 - P_{e,m})\,\beta_{0,m}^{\text{lq}} + P_{e,m}(1 - \beta_{0,m}^{\text{lq}})$.

For the considered LQ model, attempting to devise the DLMP for the cases **S1-S3** introduced in Section II-C leads to the *same fusion rule*, as shown by the following proposition.

Proposition 2: The one-bit DLMP fusion statistic based on LQ is coincident under the three different scenarios considered and equal to:

$$\Lambda_{\text{1B--DLMP}}^{\text{lq}} =$$

$$\sup_{\boldsymbol{y}_P} \frac{\sum_{m=1}^{M}(r_m^{\text{lq}} - \alpha_{0,m}^{\text{lq}})\,\Xi_m^{\text{lq}}\,d^2\left(\boldsymbol{y}_P, \boldsymbol{y}_m\right)}{\sqrt{\sum_{m=1}^{M}\alpha_{0,m}^{\text{lq}}\left[1 - \alpha_{0,m}^{\text{lq}}\right]\left(\Xi_m^{\text{lq}}\right)^2 d^4\left(\boldsymbol{y}_P, \boldsymbol{y}_m\right)}}, \quad (39)$$

where the auxiliary definition

$$\Xi_m^{\text{lq}} \triangleq \frac{(1 - 2P_{e,m})}{\alpha_{0,m}^{\text{lq}}\left[1 - \alpha_{0,m}^{\text{lq}}\right]}\,\frac{\tau_m}{\sigma_{\text{n},m}^3}\,p_{\mathcal{N}}\left(\frac{\tau_m}{\sqrt{\sigma_{\text{n},m}^2}}\right)\|\boldsymbol{h}_m\|^2 \quad (40)$$

has been employed.

Proof: The proof follows along the same lines as the RQ case and it is thus omitted for brevity. ∎

Remarks: The results in Propositions 1 and 2 prove the coincidence of DLMP rule in **S1-S3**, for *both* RQ and LQ. Accordingly, a *unique* DLMP rule will be considered in each quantization case in what follows. Also, it is worth noticing that the DLMP expressions in RQ and LQ cases retain an analogous functional dependence (see (33) and (39)), except for different expressions of the bit probability under $\mathcal{H}_0$.

The only remaining issue is how to select the quantization thresholds for RQ (collected as $\boldsymbol{\eta} \triangleq \begin{bmatrix} \eta_1 & \cdots & \eta_M \end{bmatrix}^T$) and LQ (collected as $\boldsymbol{\tau} \triangleq \begin{bmatrix} \tau_1 & \cdots & \tau_M \end{bmatrix}^T$) cases in a way to optimize DLMP performance. The aforementioned design is provided in next subsection.

C. Comparison With One-Bit GLR Counterparts

Similarly to the raw case, the one-bit DLMP-based rules reported in (33) and (39) can be implemented by performing a *grid search* w.r.t. $\boldsymbol{y}_P$ over the (limited) ROI $\mathcal{A} \in \mathbb{R}^d$. Accordingly, by denoting with $\Lambda_{\text{1B--DLMP}}$ the generic one-bit DLMP statistic, we can *approximate* it (by discretization) as follows:

$$\Lambda_{\text{1B--DLMP}}(\boldsymbol{r}) \approx \max_{j=1,2,\dots,C_P} \Lambda_{\text{LMP}}\left(\boldsymbol{r}, \boldsymbol{y}_P[j]\right). \qquad (41)$$

Accordingly, the complexity DLMP-based fusion rules is $\mathcal{O}(M\,C_P)$. This implies the same complexity reduction with respect to corresponding one-bit GLR-based counterparts. Indeed, the GLR statistic based on either RQ or LQ has an analogous expression as the raw measurement case, i.e. when replacing the pdf $p(\boldsymbol{x}; \kappa, \boldsymbol{y}_P)$ with either (the pmf) $P(\boldsymbol{r}^{\text{rq}}; \kappa, \boldsymbol{y}_P)$ or $P(\boldsymbol{r}^{\text{lq}}; \kappa, \boldsymbol{y}_P)$. For example, in the RQ case the GLR can be written as:

$$\Lambda_{\text{1B--GLR}}^{\text{rq}}(\boldsymbol{r}^{\text{rq}}) \triangleq \arg\max_{(\kappa, \boldsymbol{y}_P)} \left\{ \sum_{m=1}^{M} r_m^{\text{rq}} \ln\left(\frac{\alpha_m^{\text{rq}}(\kappa, \boldsymbol{y}_P)}{\alpha_{0,m}^{\text{rq}}}\right) \right.$$
$$\left. + (1 - r_m^{\text{rq}}) \ln\left(\frac{1 - \alpha_m^{\text{rq}}(\kappa, \boldsymbol{y}_P)}{1 - \alpha_{0,m}^{\text{rq}}}\right) \right\} \quad (42)$$

A similar expression holds for $\Lambda_{\text{1B--GLR}}^{\text{lq}}(\boldsymbol{r}^{\text{lq}})$, when replacing the bit probability $\alpha_m^{\text{rq}}(\kappa, \boldsymbol{y}_P)$ with $\alpha_m^{\text{lq}}(\kappa, \boldsymbol{y}_P)$. We observe that also in the quantized scenario Λ_{GLR} the ML estimate pair $(\hat{\kappa}, \hat{\boldsymbol{y}}_P)$ cannot be obtained in closed form. Hence, the same (joint) grid approach on $(\kappa, \boldsymbol{y}_P)$ leads to the complexity $\mathcal{O}(M\,C_P\,C_\kappa)$, where C_κ denotes the number of grid points associated to κ.

D. Design of the Local Quantizers Based on the Asymptotic Performance Analysis

In this section the local quantization thresholds at the sensors are obtained based on the semi-asymptotic analysis of the DLMP rule. Indeed, no closed-form (theoretical) expressions for detection and false-alarm probabilities exist for the DLMP test (i.e. when nuisance unobservable under $\mathcal{H}_0$ are present). A similar reasoning applies to the performance of the GLR rule in the same setup.

The asymptotic distribution of $\Lambda_{\text{1B-DLMP}}(\boldsymbol{y}_P)$, i.e. assuming $\boldsymbol{y}_P$ known, for large M is as follows [50]:

$$\Lambda_{\text{1B-DLMP}}(\boldsymbol{y}_P) \overset{a}{\sim} \begin{cases} \mathcal{N}(0,1), & \text{under } \mathcal{H}_0 \\ \mathcal{N}(\mu(\boldsymbol{y}_P),1), & \text{under } \mathcal{H}_1 \end{cases}, \quad (43)$$

where the deflection measure $\mu(\boldsymbol{y}_P) = \epsilon\sqrt{\mathcal{I}(\epsilon = 0; \sigma_s^2, \boldsymbol{y}_P)} = \sigma_s^2\sqrt{\mathcal{I}(\sigma_s^2 = 0; \epsilon, \boldsymbol{y}_P)} = \kappa\sqrt{\mathcal{I}(\kappa = 0; \boldsymbol{y}_P)}$, as the DLMP coincides in the three scenarios considered. The probabilities of detection and false alarm at the FC, using (43), can be thus expressed as follows:

$$P_D = \mathcal{Q}(\gamma_{\text{fc}} - \mu(\boldsymbol{y}_P)) \qquad P_F = \mathcal{Q}(\gamma_{\text{fc}}), \quad (44)$$

where the FC threshold can be set as $\gamma_{\text{fc}} = \mathcal{Q}^{-1}(\bar{P}_F)$ when a desired false-alarm rate $\bar{P}_F$ is given. It can be observed from (44) that increasing $\mu(\boldsymbol{y}_P)$ leads to an enlarged distance between hypotheses $\mathcal{H}_0$ and $\mathcal{H}_1$, when the POI to be detected is located at $\boldsymbol{y}_P$, i.e. for the (one-bit) position-clairvoyant LMP rule.

It can be shown that in RQ and LQ cases, respectively, the deflection equals

$$\mu_{\text{rq}}(\boldsymbol{y}_P) = \frac{\kappa}{2}\sqrt{\sum_{m=1}^{M}(\Xi_m^{\text{rq}})^2 \alpha_{0,m}^{\text{rq}}(1-\alpha_{0,m}^{\text{rq}})\, d^4(\boldsymbol{y}_P, \boldsymbol{y}_m)} \quad (45)$$

and

$$\mu_{\text{lq}}(\boldsymbol{y}_P) = \kappa\sqrt{\sum_{m=1}^{M}(\Xi_m^{\text{lq}})^2 \alpha_{0,m}^{\text{lq}}(1-\alpha_{0,m}^{\text{lq}})\, d^4(\boldsymbol{y}_P, \boldsymbol{y}_m)} \quad (46)$$

Additionally, the deflection under LQ is *twice* that under RQ. This is consistent with previous studies comparing RQ and LQ in similar (however simplified) setups.

For this reason, we aim to design the threshold vectors $\boldsymbol{\eta}$ and $\boldsymbol{\tau}$ that maximize $\mu_{\text{rq}}(\boldsymbol{y}_P)$ and $\mu_{\text{lq}}(\boldsymbol{y}_P)$, respectively, as follows:

$$\boldsymbol{\eta}^\star = \arg\max_{\boldsymbol{\eta}} \mu_{\text{rq}}(\boldsymbol{y}_P, \boldsymbol{\eta}) \quad (47)$$

$$\boldsymbol{\tau}^\star = \arg\max_{\boldsymbol{\tau}} \mu_{\text{lq}}(\boldsymbol{y}_P, \boldsymbol{\tau}) \quad (48)$$

Even if we could potentially obtain (impractical) solutions $\boldsymbol{\eta}^\star$ and $\boldsymbol{\tau}^\star$ depending on $\boldsymbol{y}_P$, for this particular problem the optimization admits an appealing solution, as summarized by the following theorem.

Theorem 1: For RQ case, the objective to be optimized for each m is $\Psi_m^{\text{rq}} \triangleq \{(\Xi_m^{\text{rq}})^2 \alpha_{0,m}^{\text{rq}}(1-\alpha_{0,m}^{\text{rq}})\}$, where:

$$\Psi_m^{\text{rq}}(\eta_m) = \frac{(1-2P_{e,m})^2}{\alpha_{0,m}^{\text{rq}}\left[1-\alpha_{0,m}^{\text{rq}}\right]} \frac{\eta_m^2}{\sigma_{\text{n},m}^6} p_{\mathcal{N}}^2\left(\frac{\eta_m}{\sqrt{\sigma_{\text{n},m}^2}}\right) \quad (49)$$

Similarly, for LQ case, the mth objective is $\Psi_m^{\text{lq}} \triangleq \{(\Xi_m^{\text{lq}})^2 \alpha_{0,m}^{\text{lq}}(1-\alpha_{0,m}^{\text{lq}})\}$, where:

$$\Psi_m^{\text{lq}}(\tau_m) = \frac{(1-2P_{e,m})^2}{\alpha_{0,m}^{\text{lq}}\left[1-\alpha_{0,m}^{\text{lq}}\right]} \frac{\tau_m^2}{\sigma_{\text{n},m}^6} p_{\mathcal{N}}^2\left(\frac{\tau_m}{\sqrt{\sigma_{\text{n},m}^2}}\right) \quad (50)$$
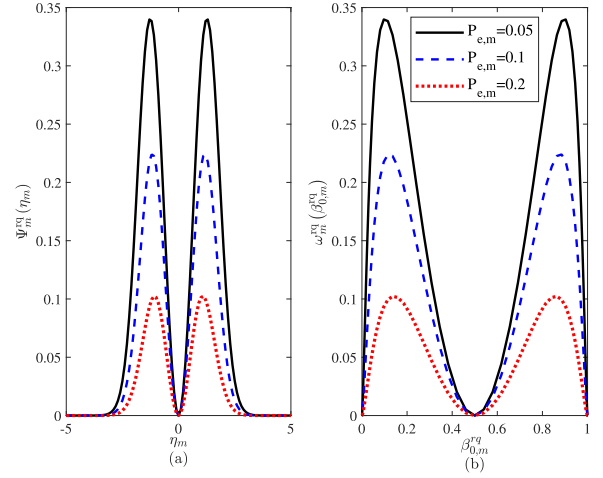
Fig. 2. (a) Ψ_m^{rq} versus η_m and (b) ω_m^{rq} versus $\beta_{0,m}^{\text{rq}}$ for $\sigma_{\text{n},m}^2 = 1$ and $P_{e,m} \in \{0.05, 0.1, 0.2\}$. The optimal quantization thresholds depend on $P_{e,m}$ value.

Proof: The proof can be readily obtained from (45) and (46) by observing that both κ and $d^4(\boldsymbol{y}_P, \boldsymbol{y}_m)$ are positive terms and are independent on the thresholds. Hence, each positive term $(\Xi_m^{\text{rq}})^2 \alpha_{0,m}^{\text{rq}}(1-\alpha_{0,m}^{\text{rq}})$ (resp. $(\Xi_m^{\text{lq}})^2 \alpha_{0,m}^{\text{lq}}(1-\alpha_{0,m}^{\text{lq}})$) should be maximized (separately) w.r.t. the corresponding threshold η_m (resp. τ_m). ∎

Remarks: first of all, the aforementioned theorem highlights that the M-dimensional design of the quantizers for the whole WSN simplifies into M *decoupled* threshold designs, whose solutions are also *independent* of $\boldsymbol{y}_P$. Hence, the optimization complexity scales linearly with the number of sensors M. By comparing the two objectives, it can be observed that they have a *similar functional dependence*. Additionally, for RQ the threshold η_m varies over the whole $\mathbb{R}$ and $\Psi_m^{\text{rq}}(\eta_m)$ is an even function. Differently, for LQ the threshold τ_m has a meaningful range of variation only over $\mathbb{R}^+$ (cf. (36)).

Such maximizations can be re-formulated in terms of the local sensing bit-probabilities (under $\mathcal{H}_0$) $\beta_{0,m}^{\text{rq}}$ and $\beta_{0,m}^{\text{lq}}$, being in bijective correspondence with η_m and τ_m, respectively, as

$$\omega_m^{\text{rq}}(\beta_{0,m}^{\text{rq}}) = \frac{p_{\mathcal{N}}^2\left(\mathcal{Q}^{-1}(\beta_{0,m}^{\text{rq}})\right)\left[\mathcal{Q}^{-1}(\beta_{0,m}^{\text{rq}})\right]^2}{\Delta_m + \beta_{0,m}^{\text{rq}}\left[1-\beta_{0,m}^{\text{rq}}\right]} \quad (51)$$

and

$$\omega_m^{\text{lq}}(\beta_{0,m}^{\text{lq}}) = \frac{p_{\mathcal{N}}^2\left(\mathcal{Q}^{-1}(\beta_{0,m}^{\text{lq}}/2)\right)\left[\mathcal{Q}^{-1}(\beta_{0,m}^{\text{lq}}/2)\right]^2}{\Delta_m + \beta_{0,m}^{\text{lq}}\left[1-\beta_{0,m}^{\text{lq}}\right]} \quad (52)$$

where $\Delta_m \triangleq [P_{e,m}(1-P_{e,m})]/(1-2P_{e,m})^2$. Since $\Psi_m^{\text{rq}}(\eta_m)$ and $\Psi_m^{\text{lq}}(\tau_m)$ (resp. $\omega_m^{\text{rq}}(\beta_{0,m}^{\text{rq}})$ and $\omega_m^{\text{lq}}(\beta_{0,m}^{\text{lq}})$) are *non-concave*, we can utilize numerical optimization routines to tackle this maximization.

In what follows, without loss of generality, we focus on the objective in (49) for the RQ case. Indeed, the objective for the LQ case ((50)) can be solved in a similar fashion. Accordingly, Fig. 2 depicts Ψ_m^{rq} versus η_m for $P_{e,m} \in \{0.05, 0.1, 0.2\}$ and unit noise variance ($\sigma_{\text{n},m}^2 = 1$). For completeness, also the re-parametrized
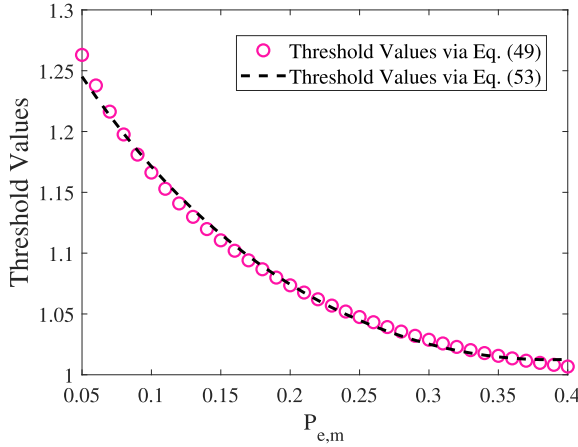
Fig. 3. Optimized threshold values $\eta_m^\star$ via (49) and (53) for different values of $P_{e,m}$.

TABLE III
OPTIMIZED THRESHOLD VALUES VIA (49) AND (53) FOR DIFFERENT VALUES OF $P_{e,m}$

$P_{e,m}$	0.05	0.1	0.15	0.2	0.3
$\eta_m^\star / \sigma_{\mathrm{n},m}$ via (49)	1.263	1.166	1.110	1.073	1.029
$\eta_m^\star / \sigma_{\mathrm{n},m}$ via (53)	1.245	1.171	1.116	1.074	1.025

objective ω_m^{rq} versus $\beta_{0,m}^{\mathrm{rq}}$ is reported. As shown in the figure, the optimum quantization threshold at each sensor clearly depends on the corresponding BEP value $P_{e,m}$ experienced. Also, $\Psi_m^{\mathrm{rq}}(\cdot)$ is an even function due to the peculiar symmetry arising from RQ. Accordingly, we can restrict our search for the optimum threshold at $\mathbb{R}^+$, as there will be always a pair of solutions $\eta_m^\star = -\eta_m^\star$ attaining the same objective value. The same observation can be drawn from inspection of $\omega_m^{\mathrm{rq}}(\cdot)$, with a symmetry around the chance probability $\beta_{0,m}^{\mathrm{rq}} = 0.5$.

By using standard curve fitting, we obtain an (approximated) equation relating the BEP and the thresholds $\eta_m^\star$ calculated optimizing the objective in (49):

$$\frac{\eta_m^\star}{\sqrt{\sigma_{\mathrm{n},m}^2}} = \frac{1}{-1.6233 P_{e,m}^2 + 1.2574 P_{e,m} + 0.7443}. \quad (53)$$

Fig. 3 compares the values of the thresholds obtained by optimizing the original objective in (49) with those calculated using (53). It is apparent that there are only slight differences between these curves. For a quantitative comparison, some relevant values from Fig. 3 are reported in Table III.

V. SIMULATION RESULTS AND DISCUSSION

In this section, we evaluate the performance of the proposed fusion rules in terms of detection (P_{D}) and false alarm probabilities (P_{F}), obtained via 10^5 Monte Carlo runs.

In the simulation setup, we assume a 2-D region, $\mathcal{A} = [0,1] \times [0,1]$, as the area to be monitored. A WSN is responsible for
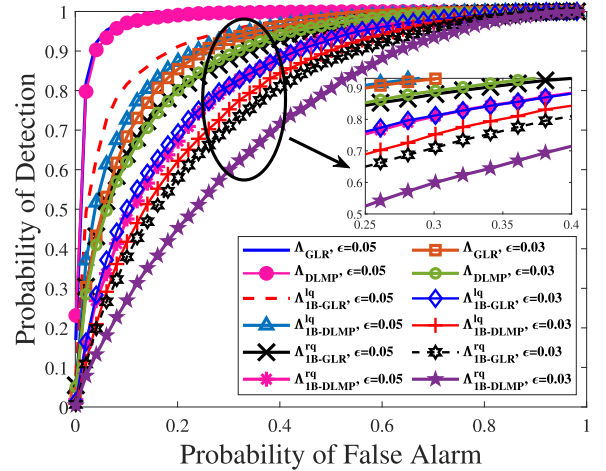
(a) PL model
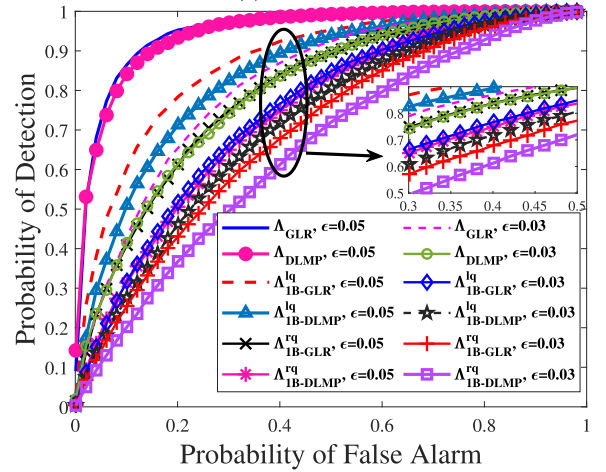
(b) EL model

Fig. 4. ROC curves of the proposed detectors, where $M = 100$, $\sigma_s^2 = 20$, $\epsilon \in \{0.03, 0.05\}$, $P_{e,m} = 0$.

detecting the presence of a POI whose position $\boldsymbol{y}_P \in \mathcal{A}$. We assume that the sensors are arranged to uniformly cover $\mathcal{A}$ in a grid fashion. Additionally, we assume that the length of sparse signal equals $K = 200$ and $\sigma_{\mathrm{n},m}^2 = 1$ for all sensors $m = 1, \ldots, M$. The elements of $\{\boldsymbol{h}_m, m = 1, \ldots, M\}$ of the compression vector are drawn from i.i.d. standard normal distributions and then normalized to satisfy $\|\boldsymbol{h}_m\|^2 = 1, \forall m$. For completeness, in what follows, we consider both PL (cf. (2)) and EL (cf. (3)) models, with parameters $\alpha = 4$ and $\beta = 0.2$ [23]. The (equivalent) signal-to-noise ratio (SNR) is given by $\mathrm{SNR} \triangleq (\epsilon \sigma_s^2)/\sigma_{\mathrm{n},m}^2 = \kappa / \sigma_{\mathrm{n},m}^2$ [28].

Based on Sections III-D and IV-C, the implementation of GLR and DLMP rules relies on grid search. Specifically, the search space of κ (for GLR only) is assumed to be $\mathcal{S}_\kappa \triangleq [0, \bar{\kappa}]$, where $\bar{\kappa}$ is such that the SNR = 20 dB. The vector collecting the points on the grid is then defined as $[0, \boldsymbol{g}_\kappa]$, where $\boldsymbol{g}_\kappa$ collects values corresponding to the SNR values -10:2.5:20 (dB). As a result, the number of bins equals $C_\kappa = 13$. Second, the search support of $\boldsymbol{y}_P$ coincides with the monitored area, i.e. $\mathcal{S}_{\boldsymbol{y}_P} = \mathcal{A}$. Accordingly, the 2-D grid is the result of sampling $\mathcal{A}$ uniformly
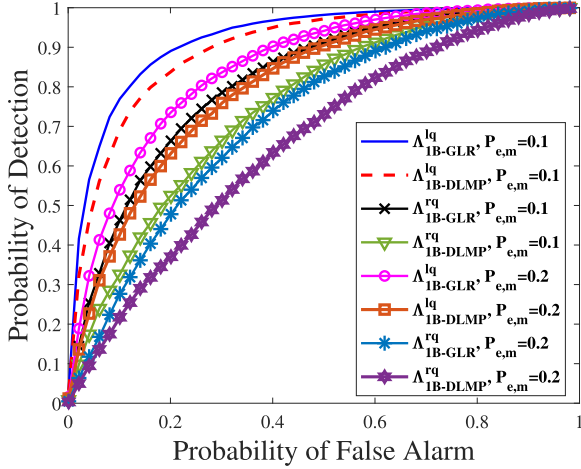
(a) PL model
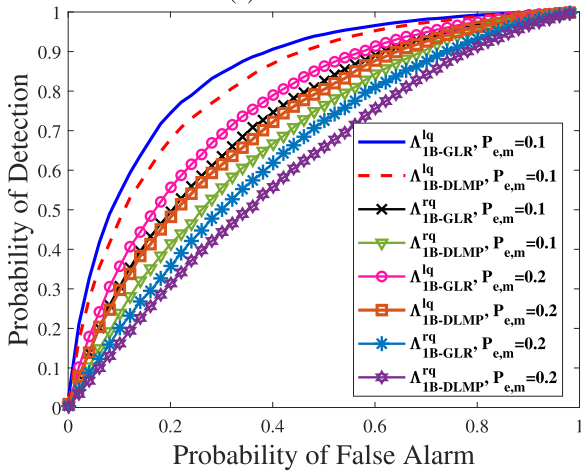
(b) EL model

Fig. 5. ROC curves of the proposed detectors, where $M = 100$, SNR $= 2$dB, $\epsilon = 0.02$, $P_{e,m} \in \{0.1, 0.2\}$.

Fig. 6. Probability of detection (P_D) at the FC vs. number of sensors M (subject to $P_\mathrm{F} = 0.05$), where SNR $= 2$ dB, $\epsilon = 0.02$, $P_{e,m} \in \{0, 0.1\}$; PL model.
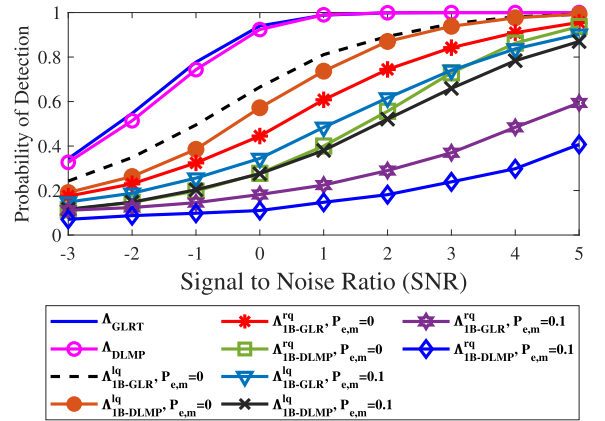
Fig. 7. Probability of detection (P_D) at the FC versus SNR (subject to $P_\mathrm{F} = 0.05$), where $M = 100$, $\epsilon = 0.02$, $P_{e,m} \in \{0, 0.1\}$; PL model.

with $C_P = N_c^2$, where $N_c = 50$. Based on the above choices, the evaluation of DLMP requires 2.5×10^3 grid points, as opposed to 3.25×10^4 points for GLR. This leads to a (more than) *ten-fold complexity reduction* of DLMP with respect to a GLR based on the same quantization strategy (or full-precision data $\boldsymbol{x}$).

Figs. 4(a) and 4(b) show the receiver operating characteristic (ROC) curves of the proposed detectors, where $M = 100$, $\sigma_s^2 = 20$, $\epsilon \in \{0.03, 0.05\}$ and $P_{e,m} = 0$ for PL and EL models, respectively. Accordingly, the equivalent SNR for $\epsilon = 0.03$ (resp. $\epsilon = 0.05$) corresponds to SNR ≈ -2dB (resp. SNR ≈ 0dB). The POI position $\boldsymbol{y}_P$ is randomly drawn according to a uniform pdf within $\mathcal{A}$. First of all, it is observed that the performance of the detectors improves by increasing the sparsity degree ϵ. Additionally, LQ proves to performs better than RQ due to the exploitation of the local LR at each sensor for both GLR and DLMP cases. Finally, GLR detectors perform slightly better than DLMP detectors in all cases.

Then in Figs. 5(a) and 5(b), we evaluate the performance of single-bit-quantized detectors via ROC under *non-ideal BSC*

with $P_{e,m} \in \{0.1, 0.2\}$, for PL and EL models, respectively. We consider a WSN with $M = 100$ sensors, SNR $= 2$ dB and $\epsilon = 0.02$. As shown in these figures, the performance of the detectors under the BSC degrades significantly by increasing the error probability of the channel. This applies to both quantization types and both detectors (GLR and DLMP) considered. Finally, the performance under EL model is generally lower than that under PL model, due to more rapid attenuation represented by the peculiar AAF.

We then investigate the performance trend of WSNs when increasing the number of sensors. Accordingly, Fig. 6 depicts the FC detection probability P_D vs. M, where the false-alarm rate is set to $P_\mathrm{F} = 0.05$. In this scenario, we consider SNR $= 2$ dB, $\epsilon = 0.02$ and $P_{e,m} \in \{0, 0.1\}$. Also, without loss of generality in what follows we focus on the PL attenuation model. It is seen that the performance of the all detectors clearly improve by increasing the number of sensors. This applies to all the considered quantization schemes and channel conditions. Still, a lower probability of error of the BSC results in a sharper trend toward ideal performance. From comparison of LQ and RQ, it is apparent that the former guarantees higher performance over
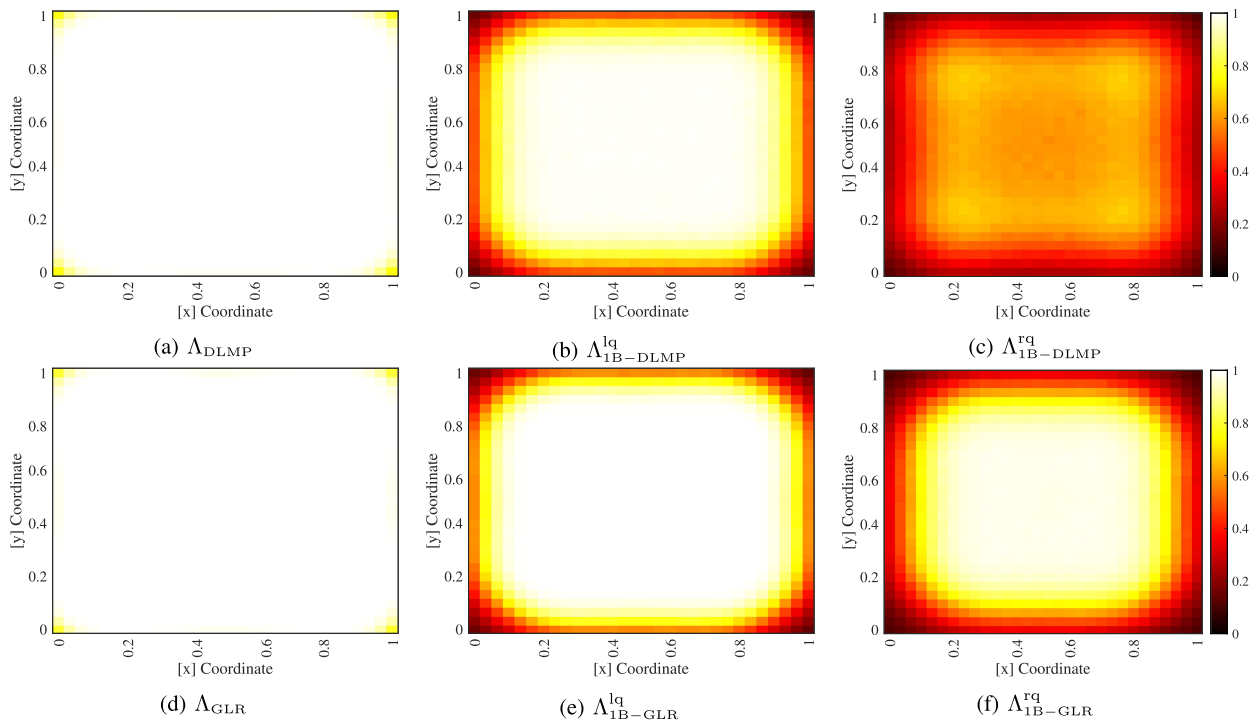
Fig. 8. P_D heatmaps vs. POI position $\boldsymbol{y}_P$ (subject to $P_\mathrm{F} = 0.05$) for (a) Λ_{DLMP}, (b) $\Lambda_{\mathrm{1B-DLMP}}^{\mathrm{lq}}$, (c) $\Lambda_{\mathrm{1B-DLMP}}^{\mathrm{rq}}$, (d) Λ_{GLR}, (e) $\Lambda_{\mathrm{1B-GLR}}^{\mathrm{lq}}$ and (f) $\Lambda_{\mathrm{1B-GLR}}^{\mathrm{rq}}$, where $M = 100$, SNR $= 2$ dB, $\epsilon = 0.02$, $P_{e,m} = 0$; PL model.

the whole considered range of WSN size. Finally, by comparing GLR and DMLP detectors, the performance loss of the latter is more significant in the RQ case, while less relevant in the (better) case of LQ.

Furthermore, we provide a complementary view of the performance w.r.t. a relevant sensing parameter of the POI. Accordingly, Fig. 7 shows the P_D versus the SNR for the proposed detectors when $P_\mathrm{F} = 0.05$. We recall that the SNR considered *jointly* takes into account both the sparsity and the signal SNR via the parameter κ. As can be observed, by increasing the SNR, the performance of the detector improves. In addition, the quality of the BSC greatly affects the performance of the proposed detectors.

Finally, in Fig. 8 we investigate the effect of POI location $\boldsymbol{y}_P$ on the probability of detection P_D of the proposed detectors (subject to $P_\mathrm{F} = 0.05$) based on full-precision/quantized data. Their perfomance is investigated by varying the position $\boldsymbol{y}_P$ over the whole ROI $\mathcal{A}$. The WSN sensing parameters considered are $\epsilon = 0.02$ and SNR $= 2$ dB. Furthermore, the size of the WSN is $M = 100$, whereas the BSCs are assumed to be ideal ($P_{e,m} = 0$) for simplicity. By looking at the results, there is an obvious performance gap between the GLR/DLMP detectors (which use full-precision observations) and 1-bit quantized detectors (either RQ- or LQ-based) over the whole ROI. Still, fusion rules based on LQ provide an overall improved detection rate. Moreover, by looking at the qualitative profile of all the heatmaps in Fig. 8, the performance of the proposed detectors degrades only at the edges of the ROI. This is the effect of the regular (grid-like) WSN placement within the ROI.

VI. CONCLUSION

In this paper, we considered DD of a localized POI via a WSN. Each sensor measures the POI absence/presence modeled as a sparse stochastic signal whose (average) signal loss depends on the POI-sensor distance. CS-based (resp. CS-based plus quantized) observations of sensors are sent to the FC via (error-prone) reporting channels where the final decision is made about the absence/presence of the POI. Because of the nuisance parameter, the LMP is not applicable and therefore the DLMP statistic was adopted to derive efficient fusion rules. It was shown that the DLMP rule *coincides* for the three considered tests of hypotheses. This applies to *both* full-precision and quantized communication scenarios.

Focusing on the (more realistic) *quantized communication scenario*, the WSN performance was further optimized by designing the sensors' quantizers. This objective was accomplished by resorting to the asymptotic performance of position-clairvoyant LMP rule associated to either to RQ or LQ. It was shown that (for both quantization types) the proposed design leads to a *sensor-decoupled* optimization, which is *independent* on the POI parameters $\{\epsilon, \sigma_s^2, \boldsymbol{y}_P\}$ and can be solved *offline* via a simple 1-D line search, see e.g. (49)–(50). Still, it was observed that each quantization threshold depends on the BEP value $P_{e,m}$ of the reporting channel associated to that sensor. Simulation results highlighted only a moderate loss of DLMP-based rules w.r.t. GLR-based rules (while being significantly *less complex*). This result is more evident in the analog case and when LQ is applied, with the loss more pronounced when RQ is adopted. Also, it was shown that both rules are able to capitalize (*a*) a

larger WSN and (*b*) stronger (and/or less sparse) emitted signal by the POI, even in the case of one-bit quantization. Still, the performance is rapidly degraded when the reporting channel deviates from (near-)ideality.

Future directions of research will include (*a*) design of multi-bit DLMP detectors for the considered sparse model, (*b*) considering the presence of non-Gaussian noise/interference [29], (*c*) taking into account dependent observations [35] (*d*) adoption of censoring sensors [52] (to further improve energy-efficiency) and (*e*) local & global rule design for sparsely-connected WSN architectures, such as tree-structured sensor networks [46] and (*f*) taking into account advanced reporting channels and explicitly considering them in the design stage (e.g. a "decode-and-fuse" approach [53]).

APPENDIX A
PROOF OF PROPOSITION 1 (EQUIVALENCE OF DLMP RULES FOR RAW QUANTIZATION IN SCENARIOS S1–S3)

To prove the equivalence in scenarios **S1–S3**, we start from the implicit forms of the corresponding DLMP detectors based on the 1-bit (error-prone) raw-quantized observations $\boldsymbol{r}^{\mathrm{rq}} \triangleq [r_1^{\mathrm{rq}}, r_2^{\mathrm{rq}}, \ldots, r_M^{\mathrm{rq}}]^T$. Accordingly, their expression is:

$$\Lambda_{1\mathrm{B-DLMP(1)}}^{\mathrm{rq}} \triangleq \sup_{(\sigma_s^2, \boldsymbol{y}_P)} \frac{\left(\frac{\partial \ln P(\boldsymbol{r}^{\mathrm{rq}}; \epsilon, \sigma_s^2, \boldsymbol{y}_P)}{\partial \epsilon} \right)\Big|_{\epsilon=0}}{\sqrt{\mathcal{I}_{1\mathrm{B}}^{\mathrm{rq}}(\epsilon=0; \sigma_s^2, \boldsymbol{y}_P)}} \quad (54)$$

$$\Lambda_{1\mathrm{B-DLMP(2)}}^{\mathrm{rq}} \triangleq \sup_{(\epsilon, \boldsymbol{y}_P)} \frac{\left(\frac{\partial \ln P(\boldsymbol{r}^{\mathrm{rq}}; \epsilon, \sigma_s^2, \boldsymbol{y}_P)}{\partial \sigma_s^2} \right)\Big|_{\sigma_s^2=0}}{\sqrt{\mathcal{I}_{1\mathrm{B}}^{\mathrm{rq}}(\sigma_s^2=0; \epsilon, \boldsymbol{y}_P)}} \quad (55)$$

$$\Lambda_{1\mathrm{B-DLMP(3)}}^{\mathrm{rq}} \triangleq \sup_{\boldsymbol{y}_P} \frac{\left(\frac{\partial \ln P(\boldsymbol{r}^{\mathrm{rq}}; \kappa, \boldsymbol{y}_P)}{\partial \kappa} \right)\Big|_{\kappa=0}}{\sqrt{\mathcal{I}_{1\mathrm{B}}^{\mathrm{rq}}(\kappa=0; \boldsymbol{y}_P)}} \quad (56)$$

where $\mathcal{I}_{1\mathrm{B}}^{\mathrm{rq}}(\epsilon=0; \sigma_s^2, \boldsymbol{y}_P)$, $\mathcal{I}_{1\mathrm{B}}^{\mathrm{rq}}(\sigma_s^2=0; \epsilon, \boldsymbol{y}_P)$ and $\mathcal{I}_{1\mathrm{B}}^{\mathrm{rq}}(\kappa=0; \boldsymbol{y}_P)$ are the relevant Fisher information terms associated to $\boldsymbol{r}^{\mathrm{rq}}$, whose definitions are analogous to those in (15), (20), and (24) for the full-precision case (and thus not reported for brevity).

In order to obtain $\Lambda_{1\mathrm{B-DLMP}}^{\mathrm{rq}}$ explicitly, we expand $\ln P(\boldsymbol{r}^{\mathrm{rq}}; \epsilon, \sigma_s^2, \boldsymbol{y}_P) = \ln P(\boldsymbol{r}^{\mathrm{rq}}; \kappa, \boldsymbol{y}_P)$ considering the independence of $\boldsymbol{r}^{\mathrm{rq}} = [r_1^{\mathrm{rq}}, r_2^{\mathrm{rq}}, \ldots, r_M^{\mathrm{rq}}]^T$ as follows:

$$\ln P(\boldsymbol{r}^{\mathrm{rq}}; \epsilon, \sigma_s^2, \boldsymbol{y}_P) = \sum_{m=1}^{M} \ln \left[P(r_m^{\mathrm{rq}}; \epsilon, \sigma_s^2, \boldsymbol{y}_P) \right]$$
$$= \sum_{m=1}^{M} r_m^{\mathrm{rq}} \ln \left[\alpha_m^{\mathrm{rq}}(\epsilon, \sigma_s^2, \boldsymbol{y}_P) \right]$$
$$+ (1 - r_m^{\mathrm{rq}}) \ln \left[1 - \alpha_m^{\mathrm{rq}}(\epsilon, \sigma_s^2, \boldsymbol{y}_P) \right] \quad (57)$$

Taking the derivative of $\ln P(\boldsymbol{r}^{\mathrm{rq}}; \epsilon, \sigma_s^2, \boldsymbol{y}_P)$ w.r.t. one of the three parameters ϵ, σ_s^2 or κ, generically denoted with a hereinafter, and setting it to zero, leads to the following *compact*

result:

$$\frac{\partial \ln P(\boldsymbol{r}^{\mathrm{rq}}; \epsilon, \sigma_s^2, \boldsymbol{y}_P)}{\partial a}\Bigg|_{a=0}$$
$$= \sum_{m=1}^{M} \frac{\partial \alpha_m^{\mathrm{rq}}(\epsilon, \sigma_s^2, \boldsymbol{y}_P)}{\partial a}\Bigg|_{a=0} \frac{(r_m^{\mathrm{rq}} - \alpha_{0,m}^{\mathrm{rq}})}{\alpha_{0,m}^{\mathrm{rq}}(1 - \alpha_{0,m}^{\mathrm{rq}})} \quad (58)$$

By means of a similar reasoning, the Fisher information terms for **S1-S3** are readily obtained as:

$$\mathcal{I}_{1\mathrm{B}}^{\mathrm{rq}}(\epsilon=0; \sigma_s^2, \boldsymbol{y}_P) = \sum_{m=1}^{M} \frac{\left(\frac{\partial \alpha_m^{\mathrm{rq}}(\epsilon, \sigma_s^2, \boldsymbol{y}_P)}{\partial \epsilon} \right)^2\Big|_{\epsilon=0}}{\alpha_{0,m}^{\mathrm{rq}}(1 - \alpha_{0,m}^{\mathrm{rq}})}. \quad (59)$$

$$\mathcal{I}_{1\mathrm{B}}^{\mathrm{rq}}(\sigma_s^2=0; \epsilon, \boldsymbol{y}_P) = \sum_{m=1}^{M} \frac{\left(\frac{\partial \alpha_m^{\mathrm{rq}}(\epsilon, \sigma_s^2, \boldsymbol{y}_P)}{\partial \sigma_s^2} \right)^2\Big|_{\sigma_s^2=0}}{\alpha_{0,m}^{\mathrm{rq}}(1 - \alpha_{0,m}^{\mathrm{rq}})}. \quad (60)$$

$$\mathcal{I}_{1\mathrm{B}}^{\mathrm{rq}}(\kappa=0; \boldsymbol{y}_P) = \sum_{m=1}^{M} \frac{\left(\frac{\partial \alpha_m^{\mathrm{rq}}(\epsilon, \sigma_s^2, \boldsymbol{y}_P)}{\partial \kappa} \right)^2\Big|_{\kappa=0}}{\alpha_{0,m}^{\mathrm{rq}}(1 - \alpha_{0,m}^{\mathrm{rq}})}. \quad (61)$$

By noticing that:

$$\frac{\partial \alpha_m^{\mathrm{rq}}(\epsilon, \sigma_s^2, \boldsymbol{y}_P)}{\partial \epsilon}\Bigg|_{\epsilon=0} = \frac{\sigma_s^2}{2} \Xi_m^{\mathrm{rq}} \alpha_{0,m}^{\mathrm{rq}}(1 - \alpha_{0,m}^{\mathrm{rq}}) d^2(\boldsymbol{y}_P, \boldsymbol{y}_m) \quad (62)$$

$$\frac{\partial \alpha_m^{\mathrm{rq}}(\epsilon, \sigma_s^2, \boldsymbol{y}_P)}{\partial \sigma_s^2}\Bigg|_{\sigma_s^2=0} = \frac{\epsilon}{2} \Xi_m^{\mathrm{rq}} \alpha_{0,m}^{\mathrm{rq}}(1 - \alpha_{0,m}^{\mathrm{rq}}) d^2(\boldsymbol{y}_P, \boldsymbol{y}_m) \quad (63)$$

$$\frac{\partial \alpha_m^{\mathrm{rq}}(\epsilon, \sigma_s^2, \boldsymbol{y}_P)}{\partial \kappa}\Bigg|_{\kappa=0} = \frac{1}{2} \Xi_m^{\mathrm{rq}} \alpha_{0,m}^{\mathrm{rq}}(1 - \alpha_{0,m}^{\mathrm{rq}}) d^2(\boldsymbol{y}_P, \boldsymbol{y}_m) \quad (64)$$

Substituting (62)–(64) into both (58) and (59)–(61) allows the evaluation of the DLMP rules in (54)–(56), thus providing the coincidence expression reported in Proposition 1. This concludes the proof.

REFERENCES

[1] R. B. Davies, "Hypothesis testing when a nuisance parameter is present only under the alternative," *Biometrika*, vol. 64, no. 2, pp. 247–254, 1977.
[2] P. K. Varshney, *Distributed Detection and Data Fusion*. New York, NY, USA: Springer-Verlag, 1997.
[3] S. H. Javadi, "Detection over sensor networks: A tutorial," *IEEE Aerosp. Elect. Syst. Mag.*, vol. 31, no. 3, pp. 2–18, Mar. 2016.
[4] D. Ciuonzo and P. S. Rossi, "Data fusion in wireless sensor networks: A statistical signal processing perspective," *IET Ser. Control, Robot. Sensors*, 2019.
[5] V. S. S. Nadendla and P. K. Varshney, "Design of binary quantizers for distributed detection under secrecy constraints," *IEEE Trans. Signal Process.*, vol. 64, no. 10, pp. 2636–2648, May 2016.
[6] A. Mohammadi, S. H. Javadi, D. Ciuonzo, V. Persico, and A. Pescapé, "Distributed detection with fuzzy censoring sensors in the presence of noise uncertainty," *Neurocomputing*, vol. 351, pp. 196–204, 2019.
[7] F. Gao, L. Guo, H. Li, J. Liu, and J. Fang, "Quantizer design for distributed GLRT detection of weak signal in wireless sensor networks," *IEEE Trans. Wireless Commun.*, vol. 14, no. 4, pp. 2032–2042, Apr. 2015.

[8] D. Ciuonzo, S. H. Javadi, A. Mohammadi, and P. Salvo Rossi, "Bandwidth-constrained decentralized detection of an unknown vector signal via multi-sensor fusion," *IEEE Trans. Signal Inf. Process. Netw.*, vol. 6, pp. 744–758, 2020.

[9] D. L. Donoho, "Compressed sensing," *IEEE Trans. Inf. Theory*, vol. 52, no. 4, pp. 1289–1306, Apr. 2006.

[10] E. J. Candès and M. B. Wakin, "An introduction to compressive sampling," *IEEE Signal Process. Mag.*, vol. 25, no. 2, pp. 21–30, Mar. 2008.

[11] M. A. Davenport, P. T. Boufounos, M. B. Wakin, and R. G. Baraniuk, "Signal processing with compressive measurements," *IEEE J. Sel. Topics Signal Process.*, vol. 4, no. 2, pp. 445–460, Apr. 2010.

[12] J. Haupt and R. Nowak, "Compressive sampling for signal detection," in *Proc. IEEE Int. Conf. Acoust., Speech, Signal Process.*, 2007, pp. III-1509–III-1512.

[13] D. Ramasamy, S. Venkateswaran, and U. Madhow, "Compressive parameter estimation in AWGN," *IEEE Trans. Signal Process.*, vol. 62, no. 8, pp. 2012–2027, Apr. 2014.

[14] T. Wimalajeewa, H. Chen, and P. K. Varshney, "Performance limits of compressive sensing-based signal classification," *IEEE Trans. Signal Process.*, vol. 60, no. 6, pp. 2758–2770, Jun. 2012.

[15] J. L. Paredes, Z. Wang, G. R. Arce, and B. M. Sadler, "Compressive matched subspace detection," in *Proc. IEEE 17th Eur. Signal Process. Conf.*, 2009, pp. 120–124.

[16] K. G. Nagananda and P. K. Varshney, "On weak signal detection with compressive measurements," *IEEE Signal Process. Lett.*, vol. 25, no. 1, pp. 125–129, Jan. 2018.

[17] A. Razavi, M. Valkama, and D. Cabric, "Compressive detection of random subspace signals," *IEEE Trans. Signal Process.*, vol. 64, no. 16, pp. 4166–4179, Aug. 2016.

[18] A. Hariri and M. Babaie-Zadeh, "Compressive detection of sparse signals in additive white Gaussian noise without signal reconstruction," *Elsevier Signal Process.*, vol. 131, pp. 376–385, 2017.

[19] E. Arias-Castro, "Detecting a vector based on linear measurements," *Electron. J. Statist.*, vol. 6, pp. 547–558, 2012.

[20] G. K. Atia, "Change detection with compressive measurements," *IEEE Signal Process. Lett.*, vol. 22, no. 2, pp. 182–186, Feb. 2015.

[21] A. Shoari and A. Seyedi, "Detection of a non-cooperative transmitter in rayleigh fading with binary observations," in *Proc. IEEE Mil. Commun. Conf.*, 2012, pp. 1–5.

[22] H. Zayyani, F. Haddadi, and M. Korki, "Double detector for sparse signal detection from one-bit compressed sensing measurements," *IEEE Signal Process. Lett.*, vol. 23, no. 11, pp. 1637–1641, Nov. 2016.

[23] D. Ciuonzo and P. S. Rossi, "Distributed detection of a non-cooperative target via generalized locally-optimum approaches," *Elsevier Inf. Fusion*, vol. 36, pp. 261–274, 2017.

[24] T. Wimalajeewa and P. K. Varshney, "Sparse signal detection with compressive measurements via partial support set estimation," *IEEE Trans. Signal Inf. Process. Netw.*, vol. 3, no. 1, pp. 46–60, Mar. 2017.

[25] B. Kailkhura, T. Wimalajeewa, and P. K. Varshney, "Collaborative compressive detection with physical layer secrecy constraints," *IEEE Trans. Signal Process.*, vol. 65, no. 4, pp. 1013–1025, Feb. 2017.

[26] X. Wang, G. Li, and P. K. Varshney, "Detection of sparse signals in sensor networks via locally most powerful tests," *IEEE Signal Process. Lett.*, vol. 25, no. 9, pp. 1418–1422, Sep. 2018.

[27] D. Ciuonzo and P. S. Rossi, "Quantizer design for generalized locally optimum detectors in wireless sensor networks," *IEEE Wireless Commun. Lett.*, vol. 7, no. 2, pp. 162–165, Apr. 2018.

[28] X. Wang, G. Li, and P. K. Varshney, "Detection of sparse stochastic signals with quantized measurements in sensor networks," *IEEE Trans. Signal Process.*, vol. 67, no. 8, pp. 2210–2220, Apr. 2019.

[29] X. Wang, G. Li, C. Quan, and P. K. Varshney, "Distributed detection of sparse stochastic signals with quantized measurements: The generalized gaussian case," *IEEE Trans. Signal Process.*, vol. 67, no. 18, pp. 4886–4898, Sep. 2019.

[30] C. Li, Y. He, X. Wang, G. Li, and P. K. Varshney, "Distributed detection of sparse stochastic signals via fusion of 1-bit local likelihood ratios," *IEEE Signal Process. Lett.*, vol. 26, no. 12, pp. 1738–1742, Dec. 2019.

[31] C. Li, G. Li, and P. K. Varshney, "Distributed detection of sparse signals with physical layer secrecy constraints: A falsified censoring strategy," *IEEE Trans. Signal Process.*, vol. 68, pp. 6040–6054, 2020.

[32] D. Ciuonzo, P. Salvo Rossi, and P. K. Varshney, "Distributed detection in wireless sensor networks under multiplicative fading via generalized score tests," *IEEE Internet Things J.*, vol. 8, no. 11, pp. 9059–9071, Jun. 2021.

[33] J. Haupt, W. U. Bajwa, M. Rabbat, and R. Nowak, "Compressed sensing for networked data," *IEEE Signal Process. Mag.*, vol. 25, no. 2, pp. 92–101, Mar. 2008.

[34] T. Wimalajeewa and P. K. Varshney, "OMP based joint sparsity pattern recovery under communication constraints," *IEEE Trans. Signal Process.*, vol. 62, no. 19, pp. 5059–5072, Oct. 2014.

[35] T. Wimalajeewa and P. K. Varshney, "Compressive sensing-based detection with multimodal dependent data," *IEEE Trans. Signal Process.*, vol. 66, no. 3, pp. 627–640, Feb. 2018.

[36] F. Li, J. Fang, H. Li, and L. Huang, "Robust one-bit Bayesian compressed sensing with sign-flip errors," *IEEE Signal Process. Lett.*, vol. 22, no. 7, pp. 857–861, Jul. 2015.

[37] S. Kafle, T. Wimalajeewa, and P. K. Varshney, "Noisy one-bit compressed sensing with side-information," 2020, *arXiv:2006.05454*.

[38] M. A. Al-Jarrah, M. A. Yaseen, A. Al-Dweik, O. Dobre, and E. Alsusa, "Decision fusion for IoT-based wireless sensor networks," *IEEE Internet Things J.*, vol. 7, no. 2, pp. 1313–1326, Feb. 2020.

[39] P. S. R. D. Ciuonzo and S. Dey, "Massive MIMO channel-aware decision fusion," *IEEE Trans. Signal Process.*, vol. 63, no. 3, pp. 604–619, Feb. 2015.

[40] C. Soussen, J. Idier, D. Brie, and J. Duan, "From Bernoulli-Gaussian deconvolution to sparse signal restoration," *IEEE Trans. Signal Process.*, vol. 59, no. 10, pp. 4572–4584, Oct. 2011.

[41] J. Ziniel and P. Schniter, "Dynamic compressive sensing of time-varying signals via approximate message passing," *IEEE Trans. Signal Process.*, vol. 61, no. 21, pp. 5270–5284, Nov. 2013.

[42] M. Korki, J. Zhang, C. Zhang, and H. Zayyani, "Iterative Bayesian reconstruction of non-IID block-sparse signals," *IEEE Trans. Signal Process.*, vol. 64, no. 13, pp. 3297–3307, Jul. 2016.

[43] C. Bazot, N. Dobigeon, J.-I. Tourneret, and A. O. Hero, "A Bernoulli-Gaussian model for gene factor analysis," in *Proc. IEEE Int. Conf. Acoust., Speech, Signal Process.*, 2011, pp. 5996–5999.

[44] F.-F. Wang and Q. H. Liu, "A Bernoulli-Gaussian binary inversion method for high-frequency electromagnetic imaging of metallic reflectors," *IEEE Trans. Antennas Propag.*, vol. 68, no. 4, pp. 3184–3193, Apr. 2020.

[45] S. Bourguignon and H. Carfantan, "Bernoulli-Gaussian spectral analysis of unevenly spaced astrophysical data," in *Proc. IEEE 13th Workshop Stat. Signal Process.*, 2005, pp. 811–816.

[46] C. Li, G. Li, and P. K. Varshney, "Distributed detection of sparse stochastic signals with 1-bit data in tree-structured sensor networks," *IEEE Trans. Signal Process.*, vol. 68, pp. 2963–2976, 2020.

[47] E. L. Lehmann and J. P. Romano, *Testing Statistical Hypotheses*. Berlin, Germany: Springer, 2006.

[48] D. Stein, "Detection of random signals in Gaussian mixture noise," *IEEE Trans. Inf. Theory*, vol. 41, no. 6, pp. 1788–1801, Nov. 1995.

[49] Y. Sung, L. Tong, and A. Swami, "Asymptotic locally optimal detector for large-scale sensor networks under the Poisson regime," *IEEE Trans. Signal Process.*, vol. 53, no. 6, pp. 2005–2017, Jun. 2005.

[50] S. M. Kay, *Fundamentals of Statistical Signal Processing: Detection Theory*, vol. 2, Englewood Cliffs, NJ, USA: Prentice Hall, Jan. 1998.

[51] S. A. Kassam, *Signal Detection in Non-Gaussian Noise*. Berlin, Germany: Springer-Verlag, 1988.

[52] C. Li, G. Li, and P. K. Varshney, "Distributed detection of sparse signals with censoring sensors via locally most powerful test," *IEEE Signal Process. Lett.*, vol. 27, pp. 346–350, 2020.

[53] D. Ciuonzo, G. Romano, and P. S. Rossi, "Channel-aware decision fusion in distributed MIMO wireless sensor networks: Decode-and-fuse vs. decode-then-fuse," *IEEE Trans. Wireless Commun.*, vol. 11, no. 8, pp. 2976–2985, Aug. 2012.

Abdolreza Mohammadi (Member, IEEE) received the B.S. degree in electrical engineering from Ferdowsi University, Mashhad, Iran, and the M.S. and Ph.D. degrees in communication systems engineering from Yazd University, Yazd, Iran. From December 2011 to June 2012, he was a Visiting Ph.D. Student with the School of Electrical and Electronic Engineering, Nanyang Technological University, Singapore. He is currently an Assistant Professor of electrical engineering with the University of Bojnord, Bojnord, Iran. His research interests include fuzzy probability, statistical signal processing, information fusion, and wireless sensor network.

Domenico Ciuonzo (Senior Member, IEEE) is currently an Assistant Professor with the University of Napoli Federico II, Naples, Italy, and the Ph.D. degree from the University of Campania L. Vanvitelli, Caserta, Italy. Since 2011, he has been holding several visiting Researcher appointments. His research interests include data fusion, statistical signal processing, wireless sensor networks, the Internet of Things, and machine learning. He is currently the Technical Editor of the IEEE TRANSACTIONS ON AEROSPACE AND ELECTRONIC SYSTEMS and the Executive Editor of the IEEE COMMUNICATIONS LETTERS. He was the recipient of two Best Paper Awards (IEEE ICCCS 2019 and Elsevier Computer Networks 2020), 2019 Exceptional Service award from IEEE AESS, 2020 Early-Career Technical Achievement Award from IEEE SENSORS COUNCIL for sensor networks/systems, and 2021 Early-Career Award from IEEE AESS for contributions to decentralized inference and sensor fusion in networked sensor systems.

Ali Khazaee received the B.S. degree in electronic engineering from Ferdowsi University, Mashhad, Iran, in 2007, and the M.Sc. and Ph.D. degrees from the Babol University of Technology, Babol, Iran, in 2010 and 2015, respectively. He is currently an Assistant Professor with the Department of Electrical Engineering, University of Bojnord, Bojnord, Iran. His research interests include signal processing and pattern recognition.

Pierluigi Salvo Rossi (Senior Member, IEEE) was born in Naples, Italy, in 1977. He received the Dr.Eng. degree (*summa cum laude*) in telecommunications engineering and the Ph.D. degree in computer engineering from the University of Naples "Federico II," Naples, Italy, in 2002 and 2005, respectively. He is currently a Full Professor and the Deputy Head with the Department Electronic Systems, Norwegian University of Science and Technology (NTNU), Trondheim, Norway. He is also a part-time Research Scientist with the Department Gas Technology, SINTEF Energy Research, Norway.

Previously, he was with the University of Naples "Federico II", the Second University of Naples, Italy, NTNU, Norway, and Kongsberg Digital AS, Norway. He held visiting appointments with Drexel University, Philadelphia, PA, USA, Lund University, Lund, Sweden, NTNU, Norway, and Uppsala University, Uppsala, Sweden. His research interests include communication theory, data fusion, machine learning, and signal processing.

Prof. Salvo Rossi was awarded as the Exemplary Senior Editor of the IEEE COMMUNICATIONS LETTERS in 2018. He has been in the Editorial Board of the IEEE OPEN JOURNAL OF THE COMMUNICATIONS SOCIETY, IEEE TRANSACTIONS ON SIGNAL AND INFORMATION PROCESSING OVER NETWORKS, IEEE SENSORS JOURNAL, IEEE COMMUNICATIONS LETTERS, and IEEE TRANSACTIONS ON WIRELESS COMMUNICATIONS.